The Canadian Mineralogist
Vol. 36, pp. 303-325 (1998)

THE FORCAREI SUR RARE-ELEMENT GRANITIC PEGMATITE FIELD AND ASSOCIATED MINERALIZATION, GALICIA, SPAIN

MERCEDES FUERTES-FUENTE[1] AND AGUSTIN MARTIN-IZARD[1]

Departamento de Geología, Universidad de Oviedo, Arias de Velasco s/n, E-33005 Oviedo, Spain

ABSTRACT

The Forcarei Sur granitic pegmatite field, in the northwestern part of the Iberian Peninsula, is an example of a zoned field whose bodies of pegmatite and pegmatite – aplite belong to different subtypes of the rare-element class. It occurs in the Galicia – Tras Os Montes zone, which consists of two domains: (1) schistose rocks and (2) granitic rocks, including two-mica peraluminous synkinematic granitic rocks. The pegmatites studied are located in the Schistose Domain, and their host rocks are the metasedimentary rocks of the Paraño Group, Silurian to Devonian in age. The metasedimentary rocks were affected by three main phases of deformation of Hercynian age, accompanied by low- to medium-pressure metamorphism, in the greenschist to amphibolite facies. The pegmatites are located in the southern area of the western flank of the Forcarei synform. The two-mica peraluminous synkinematic granites were emplaced during the third tectonic phase and formed the Western Granitic Complex (WGC), which is the western limit of this pegmatitic field. Emplacement of the pegmatites also was synchronous with the third tectonic phase. The geochemical and mineralogical characteristics of these pegmatites, their internal structure and conditions of emplacement allow us to classify them as rare-element pegmatites. From lesser to a greater degree of fractionation, we distinguish: a) barren, b) beryl type, c) beryl – columbite – phosphate subtype, d) albite – spodumene type, and e) albite type. The more evolved groups are located farthest from the WGC, which we considered as the parental granite owing to its geochemical characteristics and close spatial association. These evolved pegmatites are enriched in Be, Li, Nb, Ta, Sn and P, which are concentrated as beryl, columbite – tantalite, tantalian cassiterite, apatite and montebrasite. All these minerals appear in albitic units or in the albite-rich bands from the layered bodies. Beyond these albite-rich zones, lithium can form spodumene, depending on phosphorus activity. Most of the phosphates found are metasomatic (montebrasite, apatite, eosphorite) and formed during the sodic metasomatism or in a late hydrothermal stage that altered the phosphorus-rich feldspar; other phosphates are secondary (hydroxyl-herderite and apatite). Based of fluid-inclusion data, the pegmatitic field formed at a minimum of 3 kbars and at 550°C. A drop in pressure, from the lithostatic to hydrostatic conditions, may have occurred as a result of fluid circulation along the fractures generated by a shear zone developed at the end of the third tectonic phase.

Keywords: granitic pegmatite, rare elements, zoned pegmatitic field, fluid inclusions, phosphorus, Galicia, Spain.

SOMMAIRE

Le champ de pegmatites granitiques de Forcarei Sur, dans le secteur nord-ouest de la péninsule ibérique, offre un exemple d'un cortège zoné dans lequel massifs de pegmatite et de pegmatite – aplite sont des sous-types de la classe de pegmatites à éléments rares. Ces roches ont été mises en place dans la zone de Galice – Tras Os Montes, répartie en deux domaines, un de schistes et l'autre de roches granitiques, dont certaines sont à deux micas, hyperalumineuses et syn-cinématiques. Les pegmatites étudiées sont situées dans le domaine de schistes, les roches hôtes métasédimentaires faisant partie du Groupe de Paraño, d'âge silurien à dévonien. Ces roches ont été déformées en trois phases lors de l'orogenèse hercynienne, cause d'un métamorphisme dans le faciès schistes verts à amphibolite. Les pegmatites sont situées dans le secteur sud du flanc ouest de la synforme de Forcarei. Les granites à deux micas, hyperalumineux et syn-cinématiques ont été mis en place lors du troisième épisode et constituent le complexe granitique de l'Ouest, qui détermine la limite occidentale de ce champ de pegmatites. La mise en place des pegmatites a aussi accompagné la troisième phase tectonique. D'après les caratéristiques géochimiques et minéralogiques de ces pegmatites, leur structure interne et les conditions de leur mise en place, il s'agirait de pegmatites à éléments rares. En allant de venues moins évoluées à celles qui le sont davantage, nous distinguons: a) faciès stérile, b) type à béryl, c) sous-type à béryl – columbite – phosphate, d) type à albite – spodumène, et e) type à albite. Les groupes les plus évolués sont situés le plus loin du complexe granitique de l'Ouest, considéré comme parent à cause de ses traits géochimiques et sa proximité. Ces pegmatites évoluées sont enrichies en Be, Li, Nb, Ta, Sn et P, qui se manifestent sous forme de béryl, columbite – tantalite, cassitérite tantalifère, apatite et montebrasite. Tous ces minéraux sont développés dans les unités albitiques ou dans les couches enrichies en albite des massifs lités. Au delà de ces zones riches en albite, le lithium peut se manifester sous forme de spodumène, selon l'activité du phosphore. La plupart des phosphates seraient d'origine métasomatique (montebrasite,

---

[1] *E-mail addresses*: mercedf@asturias.geol.uniovi.es, amizard@asturias.geol.uniovi.es

apatite, éosphorite), formés au cours de la métasomatose sodique ou bien lors d'un stade hydrothermal tardif qui a altéré le feldspath rich en phosphore. Les autres phosphates (hydroxyl-herdérite et apatite) sont secondaires. Selon les inclusions fluides, le champ de pegmatites s'est formé à un minimum de 3 kbar et à 550°C. La circulation d'une phase fluide le long de fissures témoignerait d'une chute de la pression, typique des conditions lithostatiques à hydrostatiques, causée par un cisaillement vers la fin de la troisième phase tectonique.

Mots-clés: pegmatite granitique, éléments rares, champ zoné de pegmatites, inclusions fluides, phosphore, Galice, Espagne.

INTRODUCTION

In the central part of Galicia, in the northwestern region of the Iberian Peninsula, there are several occurrences of granitic pegmatites that contain minerals of rare elements such as Nb, Ta, Sn, Be and Li. The presence of some of these bodies was previously cited by Parga Pondal & Martínez Cardoso (1948), who discovered a group of spodumene-bearing pegmatites in the area. In a summary of tin metalliferous ores in Galicia Occidental, Ypma (1966) cited the presence of "pegmatite – aplites" having possible economic interest. Hensen (1967) described the mineralogy and petrography of some pegmatites being mined at the time for cassiterite and beryl. Fuertes-Fuente & Martín-Izard (1994) and Fuertes-Fuente *et al.* (1995) documented in more detail a zoned pegmatitic field in this area known as Forcarei Sur. In this paper, we describe the results of geological, geochemical, mineralogical, fluid inclusion and metallogenic studies of rare-element-enriched granitic pegmatites at Forcarei Sur.

The Forcarei Sur pegmatite field is located near the border of the provinces of Pontevedra and Orense, in an area where several pegmatitic and related aplitic rocks occur within a narrow belt of metasedimentary rocks in an approximately north–south direction. The pegmatite field is limited to the west, east and south by granites, metasedimentary rock (Forcarei synform) and granodiorite (Avion granodiorite), respectively (Fig. 1).

GEOLOGICAL SETTING

The Forcarei Sur pegmatitic field is located in the Galicia – Tras Os Montes zone (Matte 1968, Farias *et al.* 1987, Barrera *et al.* 1989, Martínez Catalán *et al.* 1996), which consists of two domains, one schistose and the other granitic. The former is composed of metamorphic rocks and the Lalín–Forcarei Unit, the southern end of the large Ordenes Complex (Barrera *et al.* 1989, Monterrubio 1991) (Fig. 1). The metasedimentary rocks include mica and quartz schist, paragneiss, quartzite, calc-silicate units and felsic metavolcanic rocks. The Lalín–Forcarei Unit, as well as the Ordenes complex, which overthrusts the other groups of the schist domain, are made up of amphibolitic gabbro, amphibolite, orthogneiss, dunite and other ultramafic rocks (Monterrubio 1991).The other groups of the schistose domain, which constitutes the parautochthon, are from the bottom to the top, the Santabaia, Nogueira and Paraño groups (Marquínez 1984, Farias *et al.* 1987). The host rock of the Forcarei Sur pegmatitic field is the Paraño Group, a thick sequence of Silurian–Devonian mica and quartz schists with some interlayed graphitic horizons (Marquínez 1984).

All of the rocks of the schist domain were affected by at least three main phases of the Hercynian Orogeny (Barrera *et al.* 1989). *D*1 is manifested in the region by a schistosity (S_1) preserved in minerals delimited by the second-phase schistosity (S_2). No folds can be attributed to *D*1. Phase *D*2 developed a regional schistosity (S_2), subhorizontal recumbent folds trending north–south, and thrust faults. During *D*3, a crenulation schistosity and N–S-trending folds, such as in the Forcarei Synform, developed with a vertical axial plane. A zone of ductile shear coeval with *D*3 affected the metasediments and granitic rocks (Barrera *et al.* 1989).

According to Martínez Catalan *et al.* (1996), the regional metamorphism occurred during the first tectonic event, before the emplacement of peraluminous granites, which took place at the end of *D*3. During the first metamorphic event, sillimanite, orthoclase and staurolite were developed in metapelites.

Most of the rocks in the region are synkinematic Hercynian granites that have been affected by at least one of the three tectonic phases of the Hercynian Orogeny (Barrera *et al.* 1989). These authors subdivided the granites into two types on the basis of petrology and geochemistry: calc-alkaline granites and two-mica peraluminous granites. The last type is synkinematic with respect to the third tectonic phase, and is subdivided into several subtypes, on the basis of textural and mineralogical characteristics: 1) two-mica biotite-rich granite, 2) moderately leucocratic two-mica granite, 3) very leucocratic two-mica granite, and 4) nonhomogeneous granite, which is a "mixture" of the other subtypes mentioned. The two-mica peraluminous granites produced a contact aureole containing andalusite and biotite.

To the south of the pegmatite field, the calc-alkaline Avion granodiorite was emplaced between the second and third tectonic phases, prior to emplacement of the two-mica peraluminous granites (Barrera *et al.* 1989). The two-mica peraluminous granite cross-cuts the earlier calc-alkaline granite.

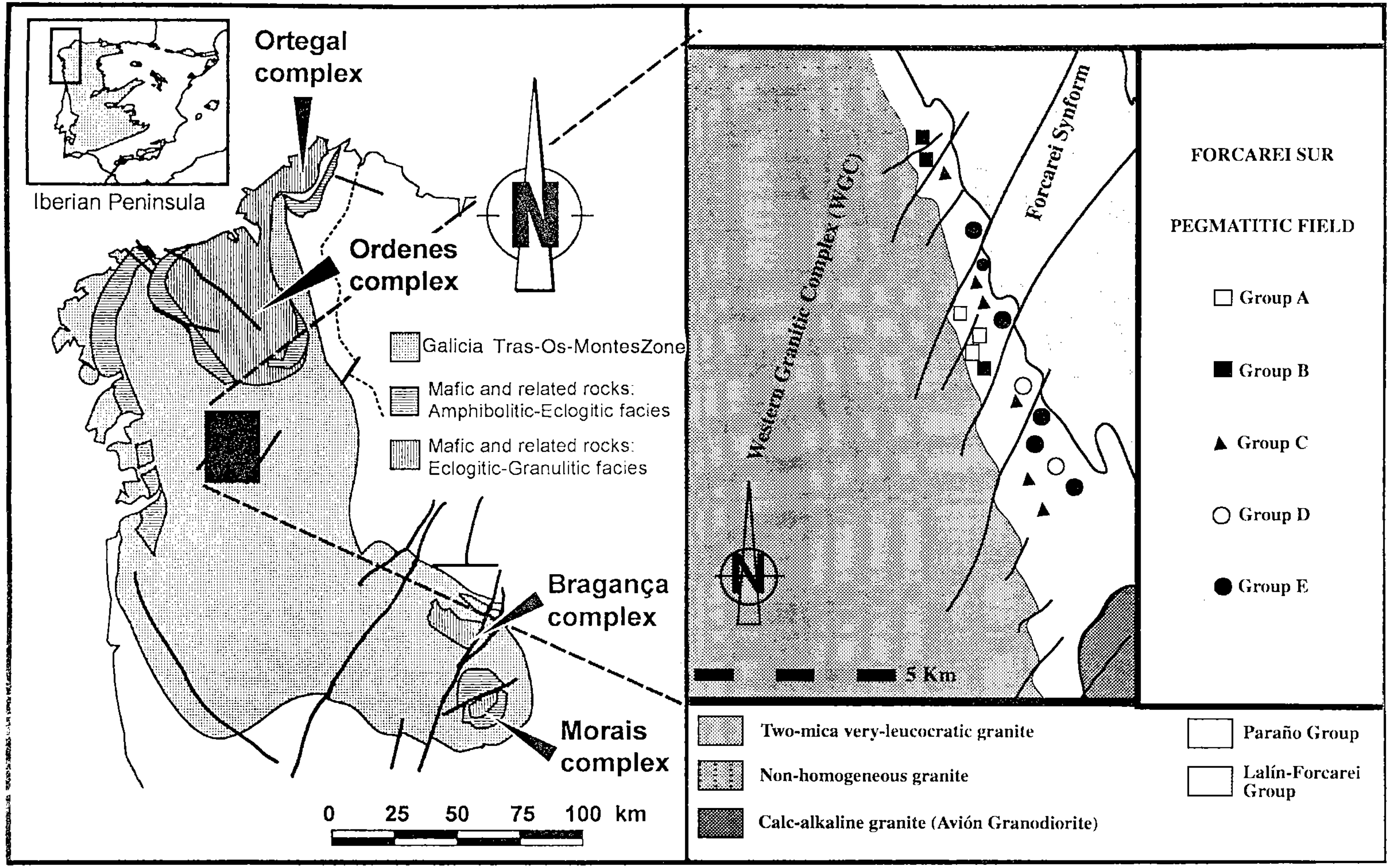

FIG. 1. Geological setting and schematic geological map of the Forcarei Sur pegmatitic field (adapted from Barrera *et al.* 1989).

TABLE 1. MAIN CHARACTERISTICS OF THE GROUPS OF PEGMATITES AND PEGMATITE–APLITES IN THE STUDY AREA

GROUPS	Main minerals	Accessory minerals	Alterations in the host rock	Morphology, internal structure and size*	Distinctive characteristics
Group A	Albite, Microcline, Quartz, Muscovite, Biotite	Garnet	New formation of muscovite, quartz and tourmaline	Irregular, bulbous masses, ellipsoidal and lenticular. No internal structure (50 × 10 m)	Not abundant; irregular shapes, contain biotite and garnet
Group B	Albite, Microcline, Quartz, Muscovite	Tourmaline, Beryl, Garnet	New formation of muscovite, quartz and tourmaline	Conform to the host rock. Dike-like No internal structure 900 × 200 m	Muscovite-rich dikes, garnet and tourmaline as dominant accessory minerals
Group C	Albite, Microcline, Quartz, Muscovite	Beryl Mn-rich apatite Eosphorite Montebrasite	New formation of muscovite, quartz, tourmaline and garnet	May or may not conform to host rock Dike-like, internal layered structure 100–800 × 5–20 m	Layered aplite–pegmatite dikes. Aplitic bands are albite-rich and thicker than pegmatitic bands Contain phosphates
Group D	Albite, Spodumene Microcline, Quartz Montebrasite Muscovite	Cassiterite Columbite–tantalite Zircon Beryl	New formation of muscovite, quartz, tourmaline and cassiterite	Conform to the host rock. Dike-like May show an internal zonal structure 100–500 × 20–100 m	Not abundant Li-bearing minerals are very abundant Albite units are present
Group E	Albite, Quartz Muscovite Microcline	Cassiterite Beryl Columbite–tantalite Mn-rich apatite	New formation of muscovite, quartz, tourmaline and cassiterite	Conform to the host rock. Dike-like Zoned structure 100–1000 × 50 m	Abundant. Internal zoned structure Albite-rich; extensive albite-rich units
Subgroup E1	Albite Quartz Muscovite	Columbite–tantalite Mn-rich apatite Zircon	New formation of muscovite, quartz and tourmaline	Conform to the host rock. Ellipsoidal Unzoned (5 × 2 m)	Scarce and small Saccharoidal albite is dominant Texture is aplitic

* (length × width).

The pegmatite field is spatially associated with a complex of two-mica peraluminous granites located to the west in Figure 1, which is referred to as "Western Granitic Complex" (WGC). However, the dominant subtype in the south-central part of this complex, where the Forcarei Sur pegmatitic field is located, is the very leucocratic two-mica granite.

DESCRIPTION OF THE PEGMATITE FIELD

The pegmatite field consists of a network of bodies of pegmatite and pegmatite – aplite within which the dimension for individual bodies of pegmatites ranges from a few meters to a kilometer in length and from less than 1 meter to 200 meters in width. The pegmatites and pegmatite – aplites strike parallel to the contact between the Paraño Group and the Western Granitic Complex and are concordant with the regional schistosity (160–180°N and subvertical dip). The pegmatitic bodies are deformed, and the degree of deformation increases from west to east. In the eastern part, they are partially mylonitized, and mylonites are preferentially developed along zones of ductile shear related to the third tectonic phase of the Hercynian Orogeny.

In all cases, the contact between the pegmatites and the host rocks is sharp and is defined by a layered rock made up of muscovite–quartz bands and thinner tourmaline-rich bands.

Five groups of pegmatite are proposed on the basis of the following characteristics: (1) size, (2) distance from the Western Granitic Complex, (3) mineralogical zoning of the different bodies, (4) textural characteristics and (5) mineralogy (Table 1).

TABLE 2. SELECTED RESULTS OF ELECTRON-MICROPROBE ANALYSES. MINERALS OF THE FORCAREI SUR PEGMATITES

Minerals	Grt	Tur^{rim}	Tur^{core}	Cst	Cst	Cst	Col-Tan	Col-Tan	Col-Tan	Col-Tan	Col-Tan	Col-Tan
(N, n)	8, 15	3, 5	3, 5	10, 18	10, 12	10, 7	10, 20	10, 22	10, 19	10, 10	10, 12	10, 15
SiO_2	36.46	37.51	37.41	-	-	-	-	-	-	-	-	-
Al_2O_3	20.23	33.16	33.46	-	-	-	-	-	-	-	-	-
FeO^{**}	28.83	12.64	12.11	0.51	0.41	1.06	12.89	12.23	12.14	2.70	6.84	10.10
MnO	13.92	0.08	0.12	0.02	0.01	0.06	8.83	9.50	9.05	11.10	8.16	7.10
SnO_2		-	-	97.12	98.71	92.43	0.43	0.40	0.74	0.55	0.81	0.28
MgO	0.31	2.30	1.87	-		-	-	-	-	-	-	-
CaO	0.19	0.07	0.01	-	-	-	-	-	-	-	-	-
Na_2O	-	1.80	1.43	-	-	-	-	-	-	-	-	-
K_2O	-	0.07	0.05	-	-	-	-	-	-	-	-	-
Ta_2O_5	-	-	-	2.15	0.34	5.50	38.24	25.18	48.85	34.40	36.18	34.66
Nb_2O_5	-	-	-	0.72	1.02	0.74	39.32	53.05	29.50	46.01	43.26	45.67
Cr_2O_3	0.01	0.11	-	-	-	-	-	-	-	-	-	-
NiO	0.03	0.03	-	-	-	-	-	-	-	-	-	-
TiO_2	0.01	0.31	0.18	0.21	0.13	0.36	0.76	-	0.50	0.63	0.73	0.64
TOTAL	100.00	88.08	86.64	100.73	100.62.	100.15	100.47	100.36	100.78	95.39	95.98	98.45

Symbols of the rock-forming minerals after Kretz (1983): Grt garnet, Tur tourmaline, Cst cassiterite, and Col-Tan columbite – tantalite. Compositions are quoted in wt.% oxides. N: number of points analyzed; n: number of crystals analyzed. FeO**: total iron expressed as FeO.

Group A: granite apophyses

These form irregular bodies 10 to 50 m in width that have an ellipsoidal to subrounded shape. Their contact with the host rock is irregular and diffuse. Tourmalinized xenoliths, in some cases partially digested, are most abundant in this group.

The granite apophyses are composed of albite, occasionally with relict patches of microcline, xenomorphic microcline, quartz and minor muscovite and biotite. Biotite is commonly intergrown with muscovite, and it is less abundant than white mica. The most abundant accessory mineral is almandine (63.6% Alm, 34.6% Sps, 1.1% Prp, 0.5% Grs) (Table 2).

The granite apophyses are characterized by random centimetric bands parallel to the host rock; these contain comb-textured microcline included in a quartz – albite – muscovite matrix.

Group B: barren pegmatites

Barren pegmatitic dikes (≤900 m in length and ≤200 m in width) consist of albite with patches of microcline, muscovite, quartz and partially albitized microcline. Centimetric beryl, idiomorphic almandine (61.4% Alm, 36.3% Sps, 1.6% Prp, 0.5% Grs) and tourmaline (schorl, ≤3 wt.% MgO, ≤2 wt.% Na_2O) are the most important accessory minerals. The tourmaline is zoned, with a blue core associated with a lower Na and Mg (Table 2), and a green rim.

Group C: albite–beryl–phosphate-bearing layered pegmatite – aplites

These bodies of pegmatite – aplite outcrop as dikes of 100 to 800 m length and 5 to 20 m width. They are characterized by alternating layers of thicker aplitic and thinner pegmatitic bands. This layered structure may be vertical and parallel to the contact with the host-rock, or horizontal and perpendicular to the contact.

The aplitic bands consist of albite, quartz, muscovite and scarce microcline corroded by albite. Idiomorphic beryl is the most abundant accessory mineral. Montebrasite, Mn-rich apatite and eosphorite also appear in lesser quantities. The pegmatitic bands are composed of microcline and quartz, in an albite and muscovite matrix.

Given that deformation was preferentialy focussed along the layers of aplite, a mineralogical banded structure is developed in the aplites, in which quartz–muscovite-rich bands alternate with quartz–albite-rich bands. In these aplitic bands, there are isolated cavities or pockets up to 2 cm in diameter, some of them with an oval shape. The formation of these cavities may be related to the deformation processes of these bodies. The pockets contain neoformed adularia, quartz, idiomorphic Mn-rich apatite and fine-grained montebrasite, or Mn-rich apatite and chlorite which do not show signs of deformation. The presence of adularia or chlorite in these cavities indicates formation from a low-temperature hydrothermal fluid.

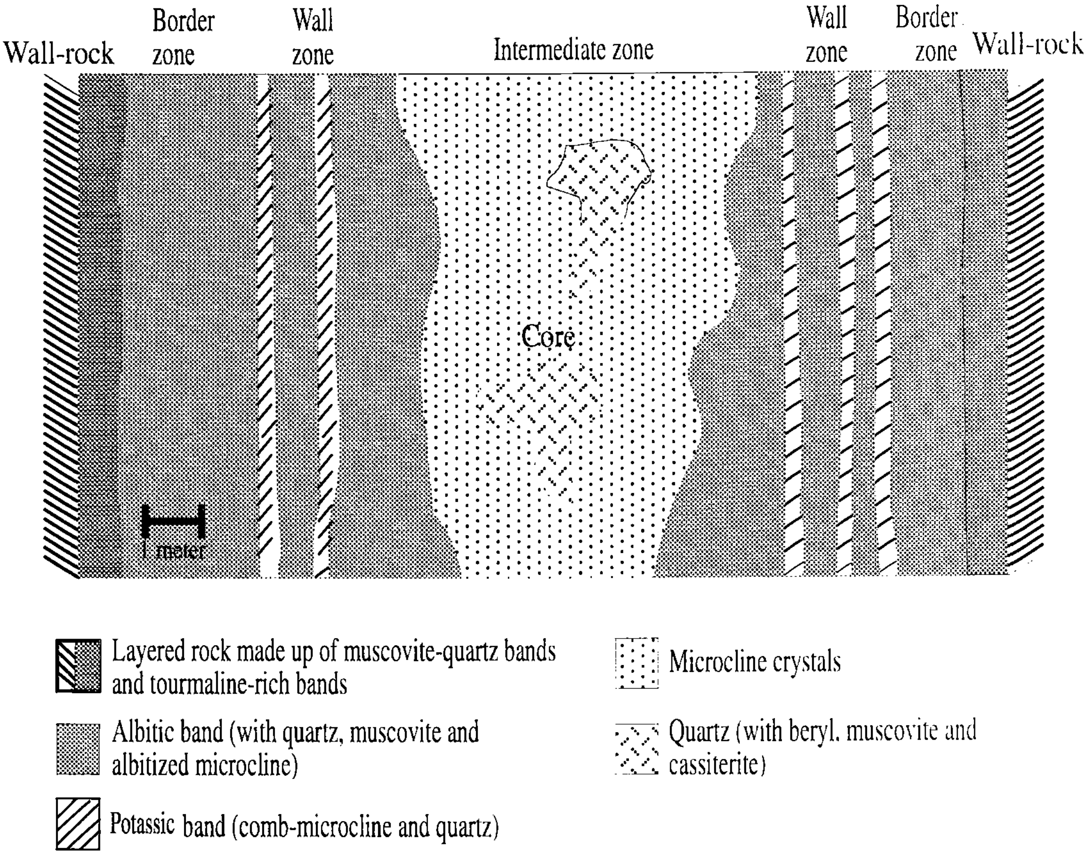

FIG. 2. Schematic representation of the internal zonation of group-E pegmatite – aplite bodies.

Group D: albite–spodumene pegmatite – aplite

Bodies of albite–spodumene pegmatite – aplite appear in the form of dikes of ≤100 to 500 m length and ≤20 to 100 m width. Their main characteristic is an internal zonal structure. The aplitic border zone consists of albite and quartz with minor spodumene partially replaced by montebrasite, muscovite and albitized microcline. Columbite–tantalite, cassiterite and zircon (Table 2) are the main accessory minerals. The inner part of the bodies is composed of two types of alternating bands, each several centimeters thick. One type contains albite, quartz, muscovite and spodumene partially replaced by montebrasite or albite. Accessory minerals include cassiterite, beryl and columbite–tantalite, which is frequently associated with montebrasite. The other type contains perthitic microcline (several centimeters in length), spodumene and quartz.

London & Burt (1982) pointed out that an increase in $\mu(PFO_2)$ and $\mu(NaLi_{-1})$ generates amblygonite plus albite from spodumene. In the case of pegmatite – aplite bodies of Group D, the lithium phosphate is montebrasite, the fluorine-poor end-member of the amblygonite–montebrasite series. This fact indicates that the role of fluorine is less important than that of phosphorus. During this replacement phenomenon, the columbite–tantalite was crystallizing, thus it appears in the neighborhood of montebrasite or albite. Owing to intensive albitization, microcline is scarce and corroded by albite.

Two bodies of group-D pegmatite – aplite, referred to as D8 and D9, have different mineralogy and texture as a result of later tectonic deformation, which defined a mylonitic fabric in these bodies. These deformed bodies of pegmatite – aplite contain mm-wide fractures filled with montebrasite. These fractures lie oblique to the orientation of the crystals. The most remarkable feature is the presence of quartz ribbons in the core of the pegmatite – aplite in association with the largest undeformed idiomorphic crystals of columbite (up to 4 cm across). This columbite–tantalite has inclusions of tantalian cassiterite and zircon. Zircon also adheres to the surface of columbite crystals. These quartz ribbons are hydrothermal in origin and are related to the deformation; thus the associated idiomorphic columbite, zircon and cassiterite crystallized during the deformation, and we consider them also hydrothermal.

Group E: albite-enriched pegmatite – aplite

Bodies of albite-enriched pegmatite – aplite, outcropping as dikes with a well-developed internal structure (Fig. 2), vary between 100 to 1000 m in length and attain 50 m in thickness. At the contact with the host rocks, these bodies of pegmatite – aplite develop a muscovite- and quartz-rich zone up to one meter thick. The aplitic border zone consists of myrmekitic albite, quartz, muscovite and albitized microcline. Abundant cassiterite (Table 2), beryl, Mn-rich apatite, columbite–tantalite and zircon all occur as accessory minerals. The wall zone consists of several bands, 8–10 centimeters in thickness, which run parallel to the contact with the host rock. They are made up of preferentially oriented microcline and quartz in an albite–muscovite matrix. The intermediate zone is made up of perthitic microcline, several centimeters in length. The core zone is composed of quartz with beryl, muscovite and cassiterite crystals.

Several smaller aplitic bodies (2 m in thickness and 5 m in length) composed of tabular albite with some quartz and muscovite are located alongside the largest bodies of pegmatite – aplite. The most important accessory mineral is columbite–tantalite, with minor beryl, Mn-rich apatite and zircon. These bodies have several cavities and veinlets. The cavities are lined with adularia, quartz, bertrandite and Fe-rich chlorite, and the veinlets are filled with hydroxylherderite and quartz. Owing to their specific characteristics, they are referred to as subgroup E1. These E1 aplitic bodies may be related to group-E pegmatite – aplite, as in Group E, some apophyses resemble subgroup E1 aplite.

In this group E, the most remarkable characteristic is the albitization of microcline and the presence of myrmekite in albite. Myrmekite forms within the albite grain and develops a rim around a core of "primitive" albite, which commonly is sericitized. In some instances, this core of "primitive" albite has a patch of microcline. Paraskovopoulos (1953) explained this texture as the result of the albitization of K-feldspar. During this process, the Si from K-feldspar forms myrmekite, and the K produces sericitization of the neoformed albite.

GEOCHEMISTRY

Whole-rock geochemistry

Representative samples of five groups and subgroups (A, B, C, D, D8, E and E1) were collected for geochemical analysis. Analytical techniques are presented in an Appendix.

All samples of pegmatite and pegmatite – aplite (Table 3) are characterized by high SiO_2 and low Fe_2O_{3t}, TiO_2, CaO and MgO content. The ratio of Na_2O *versus* K_2O is different in each pegmatitic group, and there is a trend of sodium enrichment from groups A–B to group E and subgroup E1. Thus, Na_2O/K_2O reaches values between 0.6 and 2.1 for groups A and B, whereas the rest of the groups have values up to 2.5. The pegmatites and pegmatite – aplites are peraluminous, with the ISA and A/CNK index ranging from 1.16 to 1.94 and 1.11 to 1.85, respectively. There is little difference among them owing to the low Ca contents of these bodies.

Among the trace elements, lithium has the highest concentrations in group D albite–spodumene pegmatite – aplite (4400 to 5000 ppm). Niobium and tantalum attain the highest values in groups C, D and E, from 50 to 160 ppm Nb and from 90 to 145 ppm Ta. The concentration of tin is rather variable, but group D shows the highest content, with up to 105 ppm. Cesium concentration is very low in all groups.

In order to obtain an idea about the possible parental granite, we project the ISA index *versus* A/CNK index data for the granites of the area (Barrera *et al.* 1989), which are compared with data for fertile granites from Černý (1994) (Fig. 3). The samples of very leucocratic two-mica granite (X1) plot with the fertile granites of the LCT family, whereas the calc-alkaline granite (Avion granodiorite, X2) plots in a distinctly different area. The projection of Rb, Sr and Ba in the diagram of El-Bousseily & El-Sokkary (1975) indicates that the very leucocratic two-mica granite is located in the field of highly fractionated granite. In this way, this granite may be the possible fertile parent of the pegmatites and pegmatite – aplites of Forcarei Sur. In accordance with Černý (1991), the above-mentioned major- and trace-element data allow us to include the very leucocratic two-mica granite as an LCT-type fertile granite, and we propose it as the parental granite of Forcarei Sur pegmatitic field.

Mineral chemistry

Rubidium and the other trace elements in muscovite, hafnium content in zircon and garnet composition are used as an indicator of the degree of evolution in pegmatites and help to classify the pegmatites (Černý 1991). K-feldspar also could be used, but intensive albitization in this case precludes that.

TABLE 3. REPRESENTATIVE BULK COMPOSITION OF GROUPS AND SUBGROUPS FROM THE FORCAREI SUR PEGMATITIC FIELD

	GROUP A		GROUP B		GROUP C			GROUP D			GROUP E		E1
	Pa-2	*Pa-5b*	*Pa-3*	*Pa-6*	*Pa-5a*	*Pa-7*	*Pa-12*	*Pa-8*	*Pa-8'*	*F-13*	*D-R*	*Pa-9*	*Pa-10*
SiO_2 wt.%	73.22	74.80	73.66	75.31	72.66	73.02	72.85	72.81	75.82	73.31	72.43	73.05	72.60
Al_2O_3	15.03	14.69	14.91	14.86	15.75	14.76	16.51	16.13	15.60	16.15	16.43	16.18	15.79
Fe_2O_3*	0.98	0.82	0.83	0.75	0.61	0.72	0.33	0.44	0.43	0.28	0.20	0.36	0.55
TiO_2	<0.01	<0.01	0.03	0.06	0.06	<0.01	0.05	0.04	0.01	0.01	0.05	<0.01	0.04
MgO	0.08	0.04	0.04	0.05	0.01	0.03	<0.01	0.02	0.02	0.03	0.01	<0.01	0.01
MnO	0.08	0.05	0.02	0.04	0.04	0.09	0.01	0.01	0.01	0.01	<0.01	0.01	0.02
CaO	0.44	0.24	0.31	0.34	0.69	0.46	0.19	0.35	0.24	0.09	0.17	0.35	0.43
Na_2O	3.12	4.47	3.87	4.63	6.11	4.85	6.35	6.27	3.51	5.22	8.27	7.43	6.75
K_2O	4.56	2.64	3.20	2.08	1.43	1.93	2.07	2.03	2.13	1.87	0.79	1.30	1.95
Li_2O	0.044	0.02	0.027	0.028	0.017	0.034	0.02	0.03	1.08	0.96	<0.01	0.075	0.014
Rb_2O	0.039	0.029	0.043	0.030	0.030	0.046	0.04	0.103	0.05	0.10	0.04	0.041	0.035
Cs_2O	<0.01	<0.01	<0.01	<0.01	<0.01	<0.01	<0.01	<0.01	<0.01	<0.01	<0.01	<0.01	<0.01
P_2O_5	0.42	0.24	0.31	0.29	0.61	0.48	0.12	0.23	0.24	1.55	0.32	0.37	0.36
Cr_2O_3	0.044	0.025	0.023	0.026	0.022	0.022	0.022	0.019	0.022	0.031	<0.01	0.019	0.023
L.O.I.	1.90	1.90	2.10	1.50	1.40	1.50	1.30	1.20	1.40	1.40	1.40	0.30	1.20
TOTAL	99.95	99.96	99.37	99.99	99.44	97.94	99.86	99.68	100.56	101.01	100.11	99.14	99.77
Na_2O/K_2O	0.68	1.70	1.20	2.10	4.20	2.50	3.00	3.10	1.60	2.80	10.00	5.7	3.4
ISA	1.63	1.47	1.62	1.62	1.36	1.83	1.32	1.30	1.94	1.58	1.16	1.18	1.28
A/CNK	1.38	1.38	1.53	1.51	1.23	1.36	1.29	1.24	1.85	1.55	1.14	1.14	1.11
Li ppm	207	95	125	133	81	158	92	140	5053	4460	32	350	67
Rb	362	272	399	273	274	422	364	943	500	940	367	379	319
Be	17	8	63	7	153	59	121	68	75	101	34	118	137
Nb	28	19	28	30	33	31	71	52	24	162	92	80	66
Ta	11	6	10	8	43	11	91	69	21	145	67	61	52
Sn	27	28	44	58	57	44	73	43	63	105	32	33	43
Cs	45	11	44	14	10	16	16	47	29	40	2	64	17
Sr	22	7	11	11	46	38	20	32	35	20	35	21	26
Ba	80	20	24	30	48	41	12	19	5	<3	69	3	15

The ratio Na_2O/K_2O is calculated from wt. % oxide; ISA = Al_2O_3 – (Na_2O + K_2O) and A/CNK = Al_2O_3 – (Na_2O + K_2O + CaO) are calculated using molar % oxides. * Total iron expressed as Fe_2O_3.

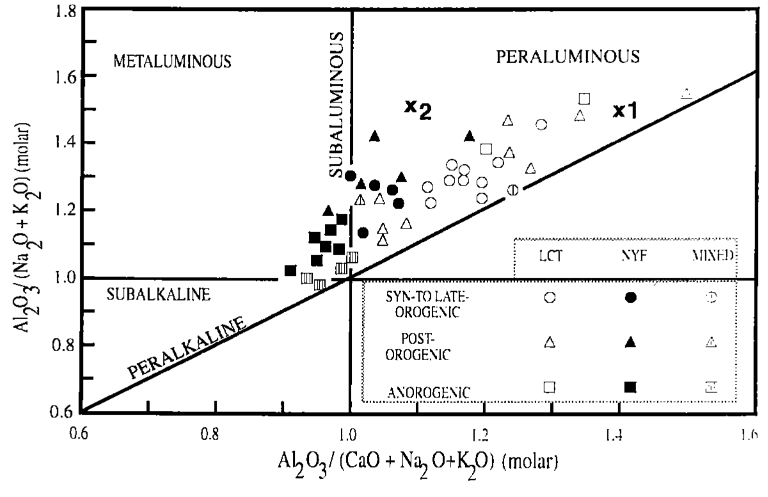

FIG. 3. Fertile granites in terms of the Shand index diagram, coded by tectonic affiliation and geochemical signature [data from Černý (1994), referring to fertile granites of LCT, NYF and mixed LCT and NYF affinity, are obtained from various localities worldwide]. Samples of possible parental granites of these pegmatites (Barrera *et al.* 1989, Gallego Garrido 1992) are plotted as X1 (very leucocratic two-mica granite) and X2 [calc-alkaline granite (Avion granodiorite)].

TABLE 4. CHEMICAL COMPOSITION OF MUSCOVITE (MAJOR ELEMENTS) FROM GROUPS MAKING UP THE FORCAREI SUR FIELD

wt% oxide	Group A	Group B	Group C	Group D	Group E
SiO_2	43.8	44.5	46.9	46.7	45.3
Al_2O_3	36.4	35.1	34.8	36.2	35.7
FeO	2.1	2.8	1.3	0.86	1.1
MnO	0.04	0.04	0.03	0.01	0.04
MgO	0.4	0.4	0.08	-	0.3
CaO	0.01	0.02	0.08	0.02	0.04
Li_2O	0.09	0.1	0.06	0.8	0.2
Na_2O	0.6	0.5	0.8	0.24	0.8
K_2O	9.3	9.2	8.7	11.3	9
Rb_2O	0.1	0.1	0.2	0.2	0.6
Cs_2O	tr.	tr.	tr.	tr.	tr.
P_2O_5	tr.	tr.	tr.	0.9	tr
Cations based on 22 Oxygens					
Si	5.98	6.08	6.32	6.07	6.16
Al(IV)	1.95	1.89	1.84	1.80	1.90
P	-	-	-	0.10	-
Sum Z	7.9	7.9	8.1	7.9	8
Al (VI)	3.90	3.78	3.68	3.70	3.81
Fe (II)	0.24	0.32	0.15	0.15	0.13
Mn	-	-	-	-	-
Mg	0.08	0.08	0.02	0.02	0.01
Li	0.05	0.06	0.03	0.03	0.11
Sum Y	4.2	4.2	3.9	3.9	4
Ca	-	-	0.01	0.01	0.01
Na	0.16	0.13	0.21	0.06	0.21
K	1.62	1.61	1.50	1.50	1.56
Rb	0.01	0.01	0.02	0.02	0.05
Cs	-	-	-	-	-
Sum X	1.8	1.8	1.8	1.6	1.8

TABLE 5. CHEMICAL COMPOSITION OF MUSCOVITE (TRACE ELEMENTS) FROM GROUPS MAKING UP THE FORCAREI SUR FIELD

ppm	Group A	Group B		Group C			Group D	Group E
Rb	570	1500	1400	1100	2000	2400	1900	5800
Cs	62	53	58	42	72	85	100	580
Sn	76	282	205	109	408	449	127	458
Nb	46	162	133	60	111	61	158	150
Ta	16	30	15	11	42	50	210	43
Li	362	438	562	206	284	184	4120	1340
P	900	220	290	1240	390	1300	3950	310
Zn	92	160	240	61	130	120	50	360
K/Rb	92.6	51.8	54.5	34.9	36.1	29.6	13.2	12.9

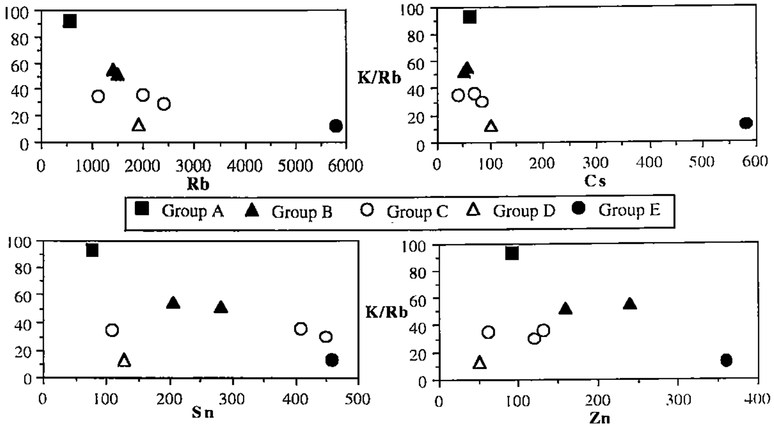

FIG. 4. The ratio K/Rb *versus* concentrations of Rb, Cs, Sn and Zn in muscovite from groups of pegmatites from the Forcarei Sur field.

The major- and trace-element concentration in muscovite from each group is shown in Tables 4 and 5. The highest Rb concentrations in muscovite are in pegmatitic group C, D and E, varying from 1100 ppm in group C to 5800 ppm in group E. Cs content increases from group C (between 42 to 85 ppm) to group E (580 ppm). The highest Li (up to 4120 ppm) and phosphorus (up to 3950 ppm) content in muscovite are in albite–spodumene pegmatites (group D). Therefore, they can be described as lithium-bearing muscovite, but not lithian muscovite. No phosphates, which could be responsible for phosphorus content, have been found as inclusions in muscovite by microscopic observation and electron-microprobe analyses; moreover, there is no positive correlation of phosphorus with Ca, indicating that micro-inclusions of apatite are not responsible for this phosphorus content. Muscovite of groups D and E shows the highest average concentration in Nb, with over 100 ppm. Zn and Sn contents are low in all muscovite separates; the highest values are found in muscovite from albite pegmatite – aplite (group E).

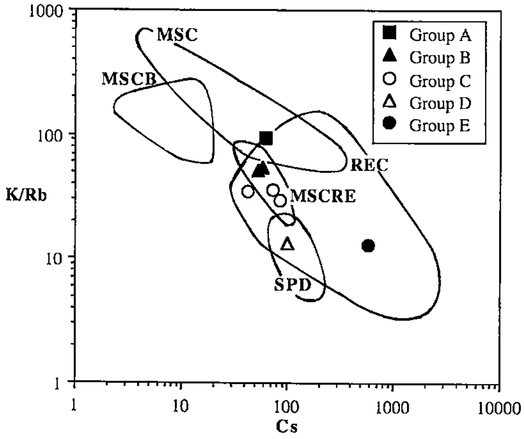

FIG. 5. The ratio K/Cs *versus* concentration of Cs in muscovite from granitic pegmatite (modified from Černý & Burt 1984). MSCB: Barren pegmatites; MSC: muscovite pegmatites; MSCRE: micaceous pegmatites rich in rare elements; REC: rare-element-enriched pegmatites, and SPD: spodumene-bearing pegmatites.

The ratios K/Rb *versus* Rb, Cs, Sn and Zn in muscovite from studied pegmatites are shown in Figure 4. The K/Rb ratio decreases and Rb concentration increases from group A to group E, indicating the same trend of fractionation established for the groups of pegmatite. Nevertheless, groups D and E have similar K/Rb values, but the higher Rb contents in muscovite of group E indicate a lower degree of evolution of Group D. The K/Rb *versus* Cs plot shows the above trend, whereas plots of K/Rb *versus* Zn and Sn show more dispersion due to the variable Zn and Sn contents in muscovite from groups B and C.

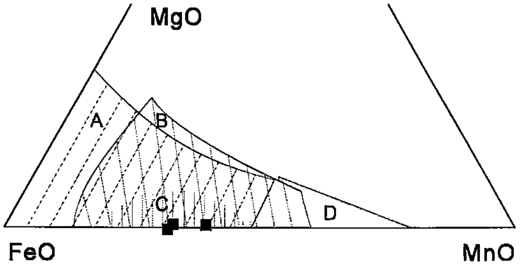

FIG. 6. Compositional fields of garnet from different types of granitic pegmatite (modified from Černý & Hawthorne 1982). A and B: muscovite-bearing pegmatite, C: muscovite-bearing, rare-element-enriched pegmatite, D: rare-element-enriched pegmatite. Square: garnet from Forcarei Sur pegmatitic field (groups A and B).

TABLE 6. REPRESENTATIVE COMPOSITION OF ZIRCON FROM THE FORCAREI SUR FIELD OF PEGMATITES

Wt.% oxide	Group B	Group D	Group D*	Group E	Sub-group E1
SiO_2	31.32	29.41	29.11	31.26	27.86
ZrO_2	64.54	57.64	58.14	61.47	54.11
HfO_2	2.256	5.46	7.80	5.10	6.83
Fe_2O_3	-	-	-	-	-
MnO	-	-	-	-	-
Al_2O_3	-	-	-	-	-
TOTAL**	98.11	92.51	95.05	97.83	89.04
Cations based on 16 oxygens					
Si		5.72	5.82	5.96	5.50
Zr	5.99	5.47	5.60	5.71	5.10
Hf	5.94	0.30	0.40	0.28	0.38
Fe(III)	0.12	-	-	-	-
Mn	-	-	-	-	-
Al	-	-	-	-	-
Ta	-	-	-	-	-
Sum	6.06	5.77	5.64	6.00	5.48

* average composition of zoned crystal of zircon.

** low totals reflect the fact that the concentration of some elements (*e.g.*, U) was not established.

Figure 5, a plot of K/Rb *versus* Cs, shows the compositional fields of muscovite from the different types of pegmatites (Černý & Burt 1984). Except for group A, all samples of muscovite from the Forcarei Sur pegmatitic field plot into the rare-element-enriched type. Muscovite from group D falls in the field of the spodumene pegmatite subtype, consistent with the mineralogical data, whereas the other compositions plot within field of the muscovite subtype of pegmatite with rare-element characteristics. Group-A muscovite lies on the boundary between the muscovite granite and rare-element-enriched pegmatite field.

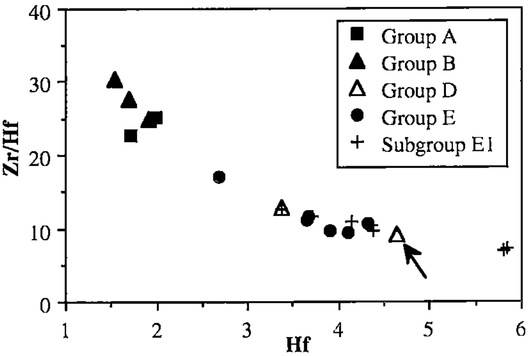

FIG. 7. The ratio Hf/Zr *versus* concentration of Zr in zircon from the groups and subgroups of granitic pegmatites from the Forcarei Sur field. Zircon associated with columbite–tantalite from group D is shown (with an arrow).

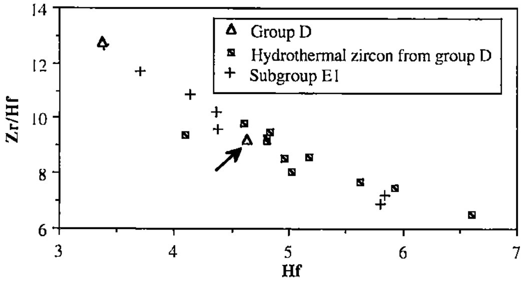

FIG. 8. The ratio Hf/Zr *versus* Zr in the hydrothermal zircon from deformed bodies of group D (D8 and D9). Moreover, zircon samples associated with columbite – tantalite from group D are shown (with an arrow). Both groups are compared to zircon from group D (not associated with the Nb–Ta oxide) and subgroup E1.

Garnet only occurs in pegmatite from groups A and B and is of almandine composition; it is not zoned (Table 2). All garnet compositions from groups A and B plot within the muscovite + rare-element-enriched fields (Fig. 6, modified from Černý & Hawthorne 1982).

Zircon was analyzed in all pegmatites except in group C, owing to its high degree of metamictization and small size. The crystals of zircon commonly are zoned, with progressive rim-to-core enrichment in Hf. Therefore, Table 6 only shows the average compositions in the case of zoned crystals.

The Zr/Hf ratio decreases in zircon from groups A and B (between 1.5 and 2 wt.% Hf) to groups D and E (between 3 and 4.5 wt.% Hf) (Fig. 7). Moreover, Hf concentrations in zircon increase from border (up to 2.5 wt.% Hf) to core (up to 4.5 wt.% Hf) of the same pegmatite body. In deformed bodies (D8 and D9) of group D, the hydrothermal zircon that is related to the quartz ribbons shows higher Hf concentrations than the rest of zircon population (Fig. 8).

The subgroup E1 contains zircon with the highest content in Hf, up to 6 wt.% Hf. Other characteristic of the zircon from E1 pegmatite – aplites is their Hf enrichment where it occurs associated with columbite–tantalite (Fig. 8).

The results of major- and trace-element chemistry of muscovite, garnet and zircon shows that the proposed groups within this pegmatitic field form an evolving series with a progressive increase in magmatic differentiation from group A to subgroup E1. Secondly, the pegmatites and pegmatite – aplites of the Forcarei Sur pegmatitic field belong to the rare-element class, and it is possible that group-A pegmatites represent the transition between muscovite granite and rare-element classes.

RARE-ELEMENT MINERALIZATION

Tin, niobium and tantalum mineralization

Tin, niobium and tantalum minerals are present in the form of cassiterite and columbite–tantalite. These minerals are disseminated in groups D, E and subgroup E1 pegmatite – aplites, and are generally concentrated in the zones richest in albite. Cassiterite also occurs in the muscovite- and quartz-rich contact zone.

Cassiterite tends to be present as twinned idiomorphic forms. It normally occurs together with columbite–tantalite, present as inclusions or coatings. The cassiterite is enriched in Ta and Nb (Nb + Ta up to 7 wt.% oxide), has low Fe, Ti and Mn, and under the microscope commonly presents oscillatory zonation, with dark bands richest in Ta, Nb, Fe, Ti and Mn (Table 2).

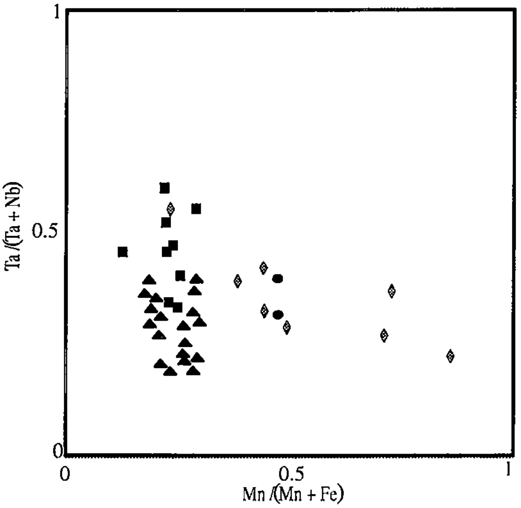

FIG. 9. Composition of the Forcarei Sur columbite – tantalite in terms of the columbite quadrilateral. Symbols: ▲: group D, ●: quartz-ribbon-rich core of D–8, deformed pegmatite – aplite, ■: group E, ◇: subgroup E1.

The columbite–tantalite forms intergrowths with cassiterite or appears as isolated crystals. Analysis of individual crystals shows compositional variation within each crystal, and each pegmatitic group has distinct compositional ranges (Table 2). An increase in Ta from group D to E was observed (Fig. 9), with a gradient from ferrocolumbite to ferrotantalite. This suggests a greater degree of fractionation in group E than group D. The columbite of subgroup E1 is rich in Mn and Nb, ranging from ferrocolumbite to manganocolumbite. A possible explanation is that subgroup E1 was formed from residual melts of group-E pegmatite – aplites. This group is the richest in cassiterite and, therefore, most of the Fe and Ta was probably extracted by this mineral, leaving a residual melt relatively rich in Mn and Nb, which led to subgroup-E1 columbite.

In the quartz-ribbon-rich core of the deformed pegmatites D8 and D9, the columbite–tantalite shows characteristics different from the columbite–tantalite previously described. The columbite–tantalite in the core of D8 and D9 is idiomorphic and appears undeformed in the middle of highly deformed quartz. In other D8 and D9 zones, the columbite–tantalite is strongly deformed and is poor in manganese. This columbite is interpreted to have a different origin (hydrothermal), probably related to deformation, which also produced the cataclastic ribbons of quartz.

TABLE 7. PHOSPHATES OF THE STUDIED PEGMATITES AND THEIR DISTRIBUTION INTO THE PEGMATITIC GROUPS OF FORCAREI SUR FIELD

Phosphates	Theoretical composition	Groups C	D	E	E1
Type A-apatite	$Ca_5(OH,F)(PO_4)_3$			+	+
Type B-apatite	"	+		+	+
Type I-montebrasite	$LiAl(F,OH)(PO_4)$	+	+		
Type II-montebrasite	"		+		
Eosphorite-childrenite	$(Mn,Fe)AlPO_4(OH)_2.H_2O$	+			
Hydroxyl-herderite	$(Ca,Mn)BePO_4(OH)$				+

Mineralization in other rare elements (Li, Be, Rb, P)

Spodumene, which has the highest concentration in group D, is the most important lithium mineral. In some bodies of groups D and C, the amblygonite–montebrasite series is also important.

Beryl is the most abundant mineral phase containing beryllium. This mineral frequently occurs in the albite-rich band of C and E bodies. The other Be minerals are hydroxyl–herderite and bertrandite. The latter appears as small and euhedral crystals with heart-shaped twins, and together with adularia fills cavities. Thus, this bertrandite occurs as a late hydrothermal mineral phase. Some of these bodies were mined for beryllium during the sixties (Hesen 1967).

TABLE 9. REPRESENTATIVE COMPOSITIONS OF EOSPHORITE FROM FORCAREI SUR PEGMATITIC FIELD

Eosphorite (Wt.% oxide)	1	2	Cations based on 8 PO4	1	2
P_2O_5	32.31	32.09	Al^{3+}	8.20	8.15
Al_2O_3	23.75	23.60	Fe^{2+}	2.65	3.09
FeO	10.72	12.60	Mn^{2+}	4.76	4.47
MnO	19.17	17.98	Mg^{2+}	-	0.02
MgO	0.00	0.05	Ca^{2+}	0.26	0.27
CaO	0.81	0.84	P^{5+}	8.00	8.00
TOTAL	86.36	87.16	ΣR^{2+}	7.67	7.85
			Fe_t/Fe_t+Mn	0.36	0.41

Muscovite is rubidium-rich, and its Rb-content is in accordance with that expected in rare-element pegmatites.

The most important phosphorus-bearing minerals in these pegmatites and pegmatite – aplites are accessory phosphates, and their distribution in the different groups is shown in Table 7. Albite and K-feldspar also contain this element (between 0.20 to 0.37 wt.% P_2O_5, as indicated by electron-microprobe analysis).

TABLE 10. REPRESENTATIVE COMPOSITIONS OF MONTEBRASITE FROM FORCAREI SUR PEGMATITIC FIELD

Montebrasite (Wt.% oxide)	Type I	Type II	Cations based on 9 (O, OH, F)	Type I	Type II
Al_2O_3	34.175	35.490	Al^{3+}	2.130	2.226
FeO	0.070	0.210	Fe^{2+}	0.030	0.009
TiO_2	0.060	0.010	Ti^{4+}	0.002	-
ZnO	0.210	-	Zn^{2+}	0.008	-
MnO	0.050	-	Mn^{2+}	0.002	-
CaO	-	0.060	Ca^{2+}	-	0.003
Na_2O	-	0.150	Na^+	-	0.043
K_2O	-	0.120	K^+	-	0.007
P_2O_5	49.500	49.580	P^{5+}	2.218	2.232
F	2.870	0.650	F^-	0.480	0.108
Sub-total	86.935	86.270	-	-	-
O=F	1.208	0.270	-	-	-
TOTAL*	85.726	86.000	-	-	-

* Low totals because lithium is not analyzed

TABLE 8. REPRESENTATIVE COMPOSITIONS OF APATITE FROM FORCAREI SUR PEGMATITIC FIELD

Apatite (Wt.% oxide)	Type A	Type B	Cations based on 26 (O, OH, F)	Type A	Type B
Al_2O_3	0.020	0.035	Al^{3+}	0.004	0.007
TiO_2	0.025	0.000	Ti4+	0.003	-
FeO	0.016	2.220	Fe^{2+}	0.002	0.318
MgO	-	0.036	Mg^{2+}	-	0.009
ZnO	-	0.018	Zn^{2+}	-	0.002
MnO	3.920	4.325	Mn^{2+}	0.585	0.647
CaO	51.400	49.150	Ca^{2+}	9.713	9.300
Na_2O	-	0.316	Na^+	-	0.108
K_2O	0.026	-	K^+	0.005	-
P_2O_5	42.000	41.924	P^{5+}	6.273	6.263
F	-	-	F^-	-	-
TOTAL	97.433	98.084			

Of these accessory phosphates, apatite is the most important. Two types of apatite, (A and B) are present. From the chemical point of view, both types are Mn-rich (Table 8). Type A appears in the core of group-E pegmatites as greenish blue euhedral crystals (≤3 cm). This type of apatite is considered primary. Type-B apatite fills cavities and veins that cut the pegmatite – aplite bodies. This mineral can occur alone or associated with other phosphates and chlorite. In other cases, apatite corrodes albite and, less commonly, microcline. This type of apatite is considered to be metasomatic.

TABLE 11. SUMMARY OF THE MICROTHERMOMETRIC DATA FOR THE DIFFERENT TYPES OF FLUID INCLUSIONS

INCLUSION TYPES	Ocurrences	Vg/Vt	$TmCO_2$	$ThCO_2$		Tmcl	Tmice	Th	
TYPE I	Group D	[10 to 40]	-	-	-	-	[-5 to -10.3]	[230 to 310]	L
		15 30					-6.5	275 310	
		185					*154*	*181*	
TYPE II	Group E	[5 to 50]	-	-	-	[10.8 to 16]	[-0.8 to -3.8]	[300 to 370]	L
		10 20				12.2 13.8	-2	300 320	
		80				*61*	*56*	*78*	
TYPE III	Group E	[60 to 90]	[-58.2 to -62]	-	-	[10.8 to 14.5]	[-1.9 to -3.8]	[340 to 400]	G
		75	-60.4			13.8	-1.8	368	C(4)
		30	*15*			*25*	*15*	*21*	L(3)
TYPE IV	Group E	[80 to 95]	[-60 to -62]	[6 to 7]	G	[11.9 to 12.8]	[-3 to -3.2]	[340 to 360]	G
		90	-60.1	6.8		12 12.8	-3	360	
		11	*11*	*11*		*11*	*11*	*11*	
TYPE V	Group E (only in apatite)	[5 to 40]	-	-	-	-	[-2.2 to -3.9]	[220 to 310]	L
		10 20					-3 -3.9	235 385	
		30					*30*	*32*	

Vg/Vt: volumetric ratio; $TmCO_2$: melting temperatures of CO_2; $ThCO_2$: homogenization temperature of CO_2, gaseous state (G), liquid state (L) and critical state (C); Tmcl: melting temperature of clathrate; Tmice: melting temperature of ice; Th: total homogenization temperature, gaseous state (G), liquid state (L) and critical state (C). All temperatures are given in °C. Range (first line), mode (second line) and number of measurements (third line, *italic*) are given for each type of fluid in each occurrence.

In all cases, these pegmatitic bodies also contain the Mn-rich member of the eosphorite–childrenite series (Table 9). It always occurs as patches distributed randomly in albite crystals; it shows irregular boundaries and corrodes the albite or fills fractures in it. These textural features indicate the metasomatic character of eosphorite.

A member of the amblygonite–montebrasite series appears in two different types, denoted I and II. Table 10 shows selected compositions, in all cases montebrasite. However, fluorine concentration in type I is higher than in type II. Type I occurs in group-C and -D pegmatite – aplites, as isolated euhedral crystals with lamellar twinning. This type is classified as primary. Type II occurs as does eosphorite, thus it is metasomatic as well. In some cases, eosphorite and type-II montebrasite appear in the same albite crystal, but form distinct patches.

Hydroxylherderite was mentioned previously as a Be-bearing mineral. In these pegmatites and pegmatite – aplites, the average result of partial chemical analyses of hydroxylherderite, indicates 42.40 wt.% P_2O_5, 33.14% CaO, 0.75% MnO and 0.23% FeO (total iron). Hydroxylherderite fills milimetric veins together with Mn-rich apatite and quartz. The hydroxylherderite can be classified as a secondary phosphate, using the terminology of Moore (1982).

FLUID INCLUSIONS

The study of fluid inclusions by microthermometry and Raman microprobe was carried out on minerals from the most highly fractionated pegmatite – aplites, which are an albite–spodumene pegmatite – aplite of group D and an albite pegmatite – aplite of group E.

The samples in group D were taken from the spodumene–montebrasite-rich core. Microthermometric measurements were possible only on quartz samples. Spodumene crystals are poorly transparent, and their fluid inclusions were either scarce or smaller than 5 μm in size. The quartz is euhedral and occurs with spodumene and montebrasite. Only one type of inclusion was observed in the quartz samples.

In group E, the samples were taken from an albitic unit, in which the rare-element minerals are concentrated. The study was carried out on two samples of apatite, three of quartz and one of beryl. This apatite belongs to type B and fills cavities or replaces albite. The apatite is greenish in the hand sample and poorly transparent. Apatite crystals commonly show irregular boundaries rich in Fe–Mn oxides, and it was not possible to study fluid inclusions in them. The rest of the crystal shows two zones, an outer one and a core. The core zone is cloudy, and the outer zone is clearer. Nevertheless, only 30 inclusions could be studied.

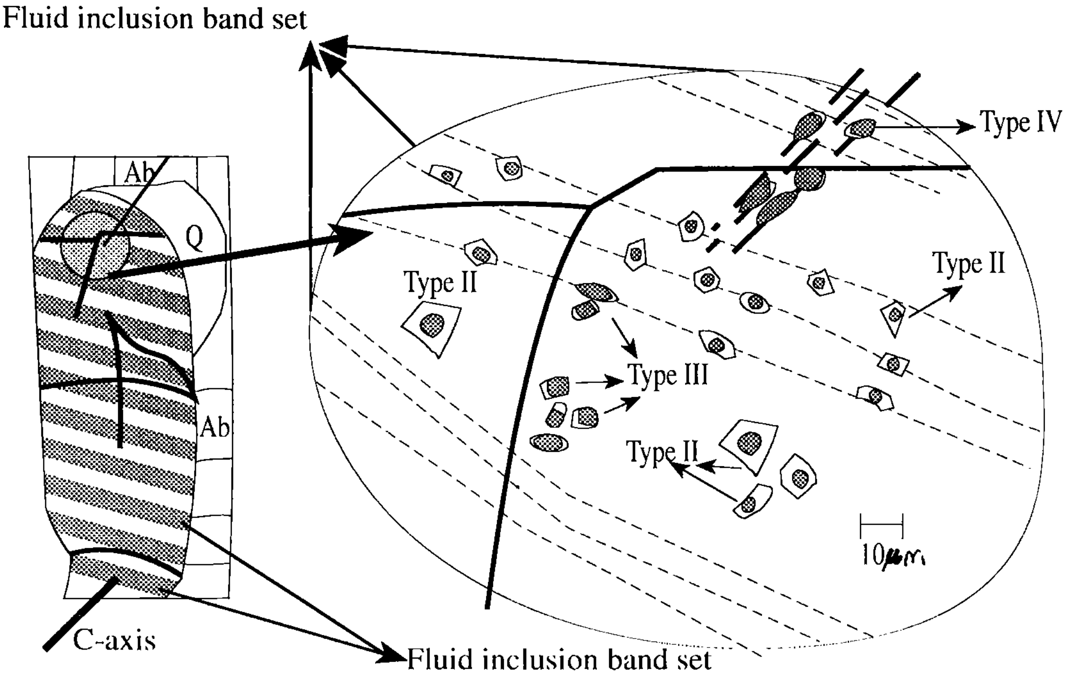

FIG. 10. Scheme of fluid-inclusion distribution in beryl sample from group-E pegmatite – aplite. Dashed lines represent fluid-inclusion band set.

Taking into account microscopic observations such as (1) the number of phases present at room temperature, (2) gas/liquid ratios, (3) microthermometric measurements and (4) Raman microprobe analyses, the fluid inclusions may be grouped into five types. Type I consist of mixed-salt aqueous inclusions; they appear only in quartz from the core of the group-D pegmatite – aplite. Types II, III and IV all are mixed-gas aqueous inclusions present in quartz and beryl from group-E pegmatite – aplite. Finally, Type V constitute low-salinity aqueous inclusions. They have only been found in apatite from group-E pegmatite – aplite. The microthermometric results are summarized in Table 11, and the microscopic observations and behavior of the fluid inclusions during heating–freezing experiments are described below.

Type-I inclusions

Most inclusions are of medium size (average between 10 and 15 µm), possess negative crystal forms of the host quartz, appear isolated or in clusters, and are generally located in the central zone of the idiomorphic quartz crystals; these inclusions are interpreted as being primary. The inclusions show two phases at room temperature, with the vapor phase occupying between 10 and 40% of the total volume of the inclusion; they commonly contain crystalline solids, interpreted to be trapped mechanically at the moment of formation of the inclusions.

The temperatures of first melting of ice vary between –35° and –50°C (the most common values are –38°C and –40°C). These temperatures are lower than the eutectic temperature of the system H_2O–NaCl (Potter & Brown 1977), and could reflect a complex salt solution (Crawford 1981). The final temperature of ice melting ranges between –5° and –10.3°C. Taking into account these temperatures and the experimental data for the system H_2O–NaCl (Bodnar 1993), an estimate of salinity ranges from 7.25 to 14 wt.% eq. NaCl.

Homogenization temperatures range between 230° and 310°C in the liquid state. The true density of this fluid cannot be calculated because the fluid composition is unknown. Nevertheless, it is possible to estimate this value assuming that the fluid present in type-I inclusions belongs to the system H_2O–NaCl. The values obtained lie between 0.75 and 0.90 g/cm^3.

Type-II inclusions

These inclusions are the most representative of quartz and beryl from group-E pegmatite – aplite. In some cases, type-II inclusions outline sets of bands that terminate abruptly a few milimeters from the crystal

TABLE 12. RAMAN DATA AND INTERPRETED BULK COMPOSITION OF SELECTED FLUID INCLUSIONS, PEGMATITE – APLITE OF THE FORCAREI SUR FIELD, AND CORRESPONDING MICROTHERMOMETRIC DATA

		MICROTHERMOMETRY						RAMAN DATA				BULK COMPOSITION					
TYPES	N°	Vg/Vt	$TmCO_2$	$ThCO_2$	Tmcl	Tmice	Th	CO_2	CH_4	N_2	dv	X H_2O	X CO_2	X CH_4	X N_2	X NaCl	D
TYPE II	PA9-2	30	-	-	12.8	-2.8	350 L	44.4	49.4	6.1	0.2	87.4	4.4	4.9	0.6	2.7	0.2
TYPE III	PA9A-1	60	-62	-	12	-2	400 G	53.2	40.2	6.6	0.2	91.4	5.0	2.8	0.8	0.6	0.1
	PA9A-2	60	-62	-	12	-2	340 G	58.12	33	8.8	0.1	92.0	4.2	3.3	0.4	0.6	0.1
TYPE IV	PA9-1	95	-60.1	6.8 G	12.8	-3	360 G	53.48	41.48	5.04	0.1	31.2	36.8	27.3	4.5	0.1	0.1

Composition are given in mole %. Vg/Vt: volumetric ratio: $TmCO_2$: melting temperatures of CO_2; $ThCO_2$: homogenization temperature of CO_2, gaseous state (G), liquid state (L) and critical state (C); Tmcl: melting temperature of clathrate: Tmice: melting temperature of ice; Th: total homogenization temperature, gaseous state (G), liquid state (L) and critical state (C). All temperatures are given in °C. dv: volatile-rich phase density; D: bulk density of inclusion.

boundary. These sets of bands lie in either one (quartz) or two directions (beryl) related to the Z axis of the two minerals in the following way: one is parallel and the other, which only appears in beryl crystals, at between 55° to 60° angles to the Z axis (from Universal stage measurements). These sets of bands could represent growth bands. In other cases, these inclusions either appear isolated or in small clusters (Fig. 10). On the basis of the criteria of Roedder (1984), these inclusions are interpreted as being primary. Inclusion morphology is variable, being polyhedral (hexagonal or prismatic), rounded, elongate or irregular. The sizes vary between 4 and 12 µm, the most common size being from 5 to 7 µm. These inclusions contain two phases at room temperature, with 20–40% vapor.

The temperature of initial melting was found to be mostly close to the stable eutectic for the system H_2O–NaCl, –20.8°C (Potter & Brown 1977). These results suggest that the aqueous solutions contain mainly Na cations in solution. The final melting temperature of ice ranges between –0.8 and –3.8°C, and the melting temperature of clathrate occurs between 10.8 and 16°C. In the microthermometric study of this type of inclusion, the presence of a volatile phase (CO_2 or CH_4) is identified only by the melting of clathrates. The salinity can be calculated from the temperature of clathrate dissociation, the melting temperature of ice and the Raman gas analyses using a clathrate stability model (Dubessy *et al.* 1992, Bakker 1995) and the computer code of Bakker (1995). The average salinity of type-II inclusions along with the Raman data are shown in Table 12.

Temperatures of homogenization, to the liquid phase, range from 300°C to 320°C.

Type-III inclusions

Type-III inclusions occur in quartz and beryl of group E pegmatite – aplites as small clusters in light zones of crystals (Fig. 10); more rarely, they appear as isolated inclusions. We consider them to be primary on the basis of the criteria of Roedder (1984). From microscopic examination, it is not possible to indicate a chronological relationship between type-III and type-II inclusions. Nevertheless, as we explain later, type II predates type III.

The morphology is variable, being polyhedral or rounded. The size of the inclusions ranges from 4 to 10 µm, and the most frequently encountered values lie between 5 and 6 µm. These show two phases at room temperature, and the vapor bubble occupies between 60 and 90% of the volume.

The melting of solid CO_2 has been measured to be between –58.2 and –62°C, but it is not possible to see the CO_2(L) meniscus because it is very narrow, and the inclusions very small or the phase change is from solid state to gaseous state. These CO_2 melting temperatures indicate the presence of significant amounts of another component (CH_4, N_2) dissolved in the CO_2 phase (Swanenberg 1979). This fact has been confirmed with Raman analyses of the gas phase in some inclusions from this type.

Where it has been possible to observe the melting of ice, the temperatures obtained range between –1.9 and –3.8°C. The melting temperature of the clathrate varies between 10.8 and 14.5°C.

Total homogenization occurs between 340 and 400°C and generally involves vapor expansion; in a few cases, homogenization is to the liquid or critical state.

Type-IV inclusions

These inclusions occur along more or less well-healed fracture planes that cross-cut several crystals; therefore, they are clearly secondary. Moreover, these fracture planes cross-cut the above-mentioned sets of bands in the quartz and beryl crystals (Fig. 10). The morphology of the inclusions is round, elongate or irregular, and the size is close to 9 µm. Two phases occur at room temperature, with the vapor bubble occupying between 80 and 95% of the volume.

During cooling, the two-phase inclusions transform into three-phase inclusions [H_2O(L) + CO_2(V) + CO_2(L)] at approximately 12°C. The carbonic phase is not pure carbon dioxide; it has melting temperatures of solid CO_2 between –60 and –62°C, which indicates the presence of other volatiles. The homogenization temperature of CO_2 varies from 6 to 7°C and occurs to the gas phase, indicating a low density of the enclosed carbonic phase. The final melting of ice occurs at approximately –3°C. The final melting of the clathrate occurs at between 11.9 and 12.8°C, after CO_2 homogenization. Total homogenization temperatures range between 340 and 360°C, to the gaseous state.

Type-V inclusions

This type of inclusion only appears in apatite from group-E pegmatite – aplite and is distributed in two manners: 1) In cloudy areas in the core of apatite crystals, where the inclusions occur aligned along two oblique directions, probably cleavage planes of the apatite. The prismatic inclusions have two phases at room temperature, with the vapor phase occupying 15 to 20%. Sizes range from 5 to 10 µm, but the most frequently encountered value is 5 µm. 2) In the clear outer zone of the apatite crystals, where the inclusions appear isolated, with a rectangular or a square outline. The inclusions contain two phases, with the vapor phase between 30 and 40% of the total volume. They vary in size between 15 and 20 µm.

All these inclusions are considered to be primary. In the clear zones of apatite crystal, where the rectangular inclusions appear, they are localized near important fractures of the crystal or close to the Mn-rich rim of the apatite crystals. Thus, we consider that the clear zones result from later growth on a older apatite core, where the inclusions occur in oblique planes. The two groups of inclusions thus probably were not formed simultaneously; the inclusions aligned along planes predate the isolated inclusions in the clear zones.

Temperatures of first melting of ice vary between –48 and –50°C. These temperatures are close to the eutectic temperature in the system H_2O–$CaCl_2$ (–49.8°C: Crawford 1981). Thus, the most probable solute in the aqueous fluid trapped in the apatite inclusions is $CaCl_2$. The final melting of ice ranges between –2.2 and –3.9°C. Total homogenization temperatures range between 220 and 310°C, to the liquid state.

The salinity and density of these inclusions have been calculated using the final melting of ice and total homogenization temperatures for the H_2O–$CaCl_2$ system with reference to the experimental data of Zhang & Frantz (1987). The salinity is low, ranging between 3.7 and 6.5 wt% $CaCl_2$, and the density varies between 0.75 and 0.90 g/cm^3.

Raman spectrometry and conditions of trapping

Several aqueous-carbonic inclusions in quartz and beryl representative of volatile-rich types (II, III and IV) were analyzed by Raman microprobe.

The density and composition of rich-volatile phase and the overall composition and density of the different types of inclusions are shown in Table 12. Raman spectrometry showed that the gaseous phase of three types of inclusions consists of CO_2 and CH_4; CH_4 is dominant in inclusions of type II, and CO_2, in inclusions of type III and IV. Only a small amount of N_2 is present (Table 12). The gaseous phase has a low density, in agreement with microthermometric observations.

The three types of volatile-bearing fluid inclusions exhibit a small decrease in the volatile phase density and increase in CO_2 content from type II to types III and IV. The overall composition of these different types of inclusion shows a decrease in the proportion of H_2O in the later volatile-rich fluids (type IV), at constant CO_2/CH_4 ratio.

P–T estimations

The representative isochores of the established aqueous-carbonic inclusion types were modeled for the system H_2O–CO_2–CH_4 using the equations of state of Kerrick & Jacobs (1981) and Jacobs & Kerrick (1981). For aqueous inclusions, the representative isochores have been drawn in the systems H_2O–NaCl and H_2O–$CaCl_2$ using the data from Zhang & Frantz (1987).

In group-D pegmatite – aplite, only type-I inclusions appear. The representative isochores are given in Figure 11, along with the stability fields of lithium aluminosilicates (London 1984) and aluminosilicates (Robie & Hemingway 1984). These isochores are approximate because they are modeled for the system H_2O–NaCl. The P–T conditions of trapping may be constrained by the mineral assemblage. The metasedimentary rocks of the Paraño Group, into which these pegmatites were emplaced, have been affected by heating due to the emplacement of the parental granite (WGC) of this pegmatite field; this metamorphism developed andalusite and biotite. From textural characteristics of the spodumene, this mineral is primary and cogenetic with the quartz that we sampled. Thus, the isochores can be projected onto the stability fields of spodumene and andalusite to calculate the conditions of trapping of the fluid in group-D pegmatite – aplite. The possible conditions of pegmatite – aplite formation were approximately 3 kbar and 550°C.

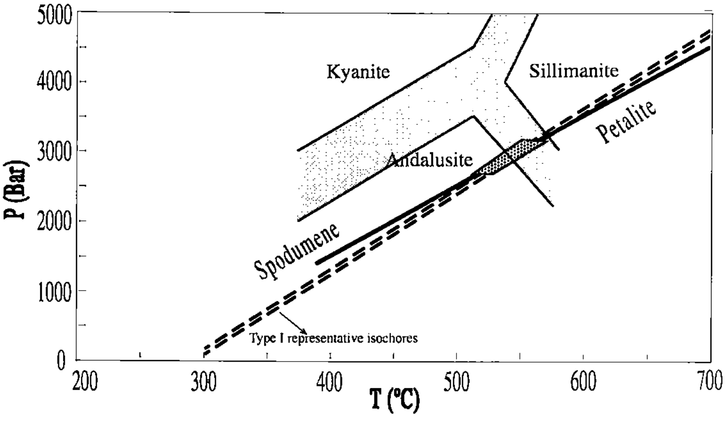

FIG. 11. P–T reconstruction for fluid inclusions (type I) of group D. The stability fields of spodumene and petalite (London 1984) are shown (solid line). The shaded area represents the possible P–T conditions of trapping of type-I inclusions. The fields of stability of the aluminosilicates (Robie & Hemingway 1984) are shown.

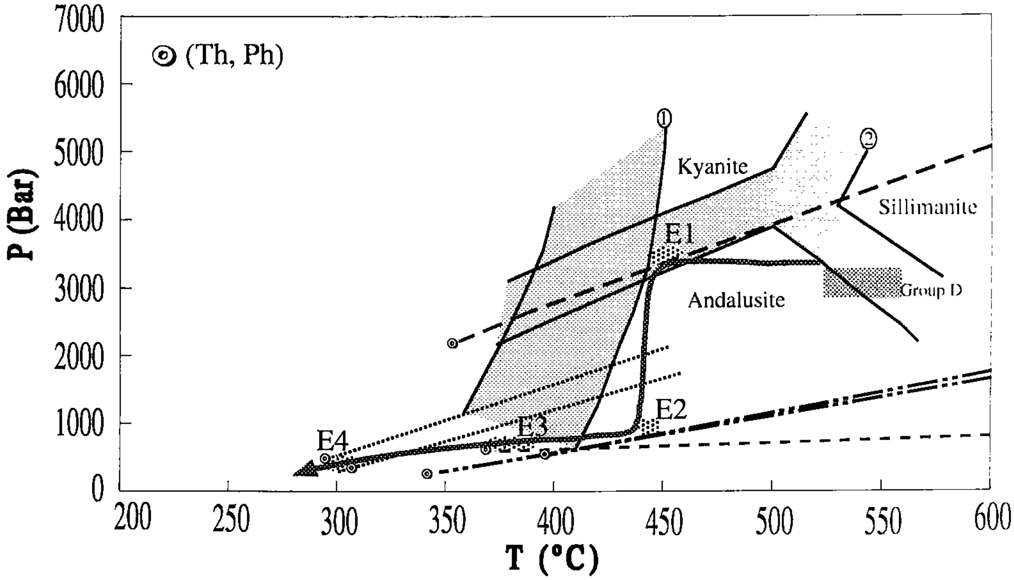

FIG. 12. P–T reconstruction with the isochores representative of the different types of fluid inclusions of group-E pegmatite – aplite. The stability fields of biotite (1) (Winkler 1976, Yardley 1989) and aluminosilicates (2) (Robie & Hemingway 1984) are shown. The dark zones are the minimum P–T conditions of trapping of inclusions of type II (– –), III (— - - —), IV (- - - -) and V (........) for the different stages (E1, E2, E3 and E4). The open circle on the isochore represents the temperature and pressure of homogenization. The grey box represents the established conditions of emplacement of group-D pegmatite – aplite (from Fig. 11). The P–T evolution of the pegmatite – aplite bodies studied is shown by the heavy line.

The representative isochores of the different types of inclusions found in group-E pegmatite – aplite (types II, III, IV and V) are shown in Figure 12. From these isochores, four stages of fluid circulation have been established in this group of pegmatite – aplite.

The first stage (E1) is represented by trapping of fluid inclusions belonging to type II. The minimal conditions of trapping are those given by the Th (total homogenization temperature) and Ph (homogenization pressure) pair, which is 350°C and 2250 bars. As mentioned above, the P–T conditions of trapping may be constrained by the mineral assemblage. Thus, the presence of biotite, formed in the Paraño Group during the emplacement of this pegmatite – aplite, indicates a minimum temperature between 360° and 410°C, taking into account the broad stability-field of biotite (Winkler 1976, Yardley 1989). Using the conditions of maximum stability and the representative isochore of type-II inclusions, minimum pressure and temperature conditions of 2.6 kbars and 375°C or 3.2 kbars and 440°C can be established for the first stage. These P–T conditions agree with the presence of andalusite in the metasedimentary rocks (Fig. 12).

The second stage (E2) of pegmatite formation was characterized by type-III inclusions. The minimum conditions of trapping (Th–Ph) lie between 340 and 400°C and 250–500 bars pressure. From a textural point of view, it was not possible to determine precisely the relative chronology between type-II and -III inclusions. We consider the trapping of type II to be very close to the trapping of type III. Thus, the entrapment temperature of type-III inclusion is considered to be similar to that of type II and within of the stability field of biotite. As we assume a temperature for this second stage similar to the temperature of the first stage, we can use the above-mentioned stability field of biotite. Thus, the estimations of the P–T pairs for stage E2 lie between 0.5 and 0.8 kbar pressure and between 375° and 440°C. Taking into account the homogenization temperatures of type-II fluid inclusions (Th = 400°C), we consider the upper limit indicated as more realistic (0.8 kbar and 440°C). In the same way, we can extend this consideration to the previously mentioned stage (E1); in the case of E1, the pressure at 440°C was 3.2 kbars.

During the third stage (E3), trapping of the later volatile-rich aqueous fluid occurred. This stage (E3) is represented by type-IV inclusions, characterized by a low-density fluid with a representative isochore close to horizontal. Thus, they show a minimum pressure of trapping close to the true pressure, between 0.5 to 0.75 kbars. For a representative isochore of type-IV inclusions, the minimum P–T conditions (Th–Ph) of trapping are 360°C and 0.6 kbar.

Finally, a last stage (E4) of circulation of a saline-aqueous (type V) fluid was established. The two representative isochores of low-salinity aqueous inclusions from apatite (type V) (Fig. 12) indicate minimum conditions of trapping (Th–Ph) between 285° and 310°C and between 0.3 and 0.6 kbars, respectively. This fluid, present in apatite, may represent an external fluid that has undergone exchange with the pegmatite body. This aqueous fluid was probably able to transport Mn and Fe, thus forming the Fe–Mn oxides that occur at the border of these apatite crystals. Moreover, the same aqueous fluid may have altered the phosphorus-rich feldspars, forming aluminophosphates with manganese and iron, such as eosphorite or type-B apatite, which appears corroding albite in the albitic units of group-E pegmatite – aplite.

Discussion and Conclusions

The Forcarei Sur pegmatitic field is made up of several bodies that are concordant with the regional schistosity that affected the Paraño Group. The pegmatitic bodies are deformed, and the degree of deformation increases from west to east. In the eastern part, they are partially mylonitized. The mylonites are preferentially developed along zones of ductile shear related to the third tectonic phase of the Hercynian Orogeny.

Five groups of pegmatite have been proposed from field observations, taking into account the shape, the size, the zoning of the different bodies, the mineralogy and the textural characteristics: A or granite apophyses, B or barren pegmatites, C or albite – beryl – phosphate-bearing pegmatite – aplite, D or spodumene – albite pegmatite – aplites, and E or albite pegmatite – aplites.

Group A is the nearest to the Western Granitic Complex, and B, C, D and E are progressively further from the contact. This distribution agrees with the increase in degree of differentiation, which progresses from west to east. The more evolved groups, D and E pegmatite – aplites, have the highest contents of rare elements (lithium, beryllium, niobium, tantalum, rubidium and tin). Moreover, they are Na-rich and Si-poor. After crystallization of most of these pegmatites, a residual Na-rich, SiO_2-depleted melt seems to have developed. The rare-element cations, which in groups D and E are Nb, Ta, Sn, Be, (Zr, Hf), together with B and P as anionic species, are concentrated in the residual sodic melt, which will tend to crystallize as fine-grained albite with cassiterite, columbite–tantalite, beryl and zircon. The boron and phosphorus are consumed in the formation of tourmaline and apatite, respectively. The presence of albite replacing microcline and spodumene (Wood & Williams-Jones 1992) and the myrmekitic textures in albite (Paraskovopoulos 1953) may indicate that the role of sodic metasomatism is very important in the internal evolution of these bodies. The small bodies near the larger group-E pegmatite – aplites are classified as subgroup E1, which is the most differentiated and mainly composed of albite. We consider subgroup E1 as having originated from residual melt of group E.

This fact is based on the results of columbite–tantalite geochemistry and their spatial relation to group-E bodies. In this case, it is probable that the residual Na-rich, SiO_2-depleted melt will form the isolated bodies that have been classified as subgroup E1.

The whole-rock geochemical results of the Forcarei Sur pegmatites indicate they are peraluminous, sodium-rich and have low concentration of Ca, Mg, Mn, Fe and Ti. The enrichment in sodium of the more evolved bodies is due to the abundance of albitic units in them or, as happens with subgroup-E1 pegmatite – aplites, these units constitute in themselves independent bodies. The albitic units are enriched in columbite–tantalite, tantalian cassiterite, beryl, apatite and, especially in group D, in lithium and phosphorus, forming montebrasite. The enrichment of some of these pegmatite – aplites in the rare elements mentioned above, together with the geochemical results in garnet and muscovite, enabled us to classify the Forcarei Sur pegmatites as rare-element-enriched pegmatites (Černý 1991).

Taking into account their geochemical characteristics and spatial position, the fertile granite proposed as the parental pluton is the very leucocratic two-mica granite that outcrops in the south-central part of the Western Granitic Complex. This type of two-mica granite shows the characteristics of fertile granites belonging to the LCT family that generates rare-element-enriched pegmatites.

On the basis of rare-element-enriched pegmatite types proposed by Černý (1991), we classify group A, the nearest to the Western Granitic Complex, as barren pegmatites, group B as beryl pegmatites, group C also belongs to the beryl type, but of the subtype beryl – columbite – phosphate pegmatites, although columbite has not been found, group D belongs to albite – spodumene type, and group E belongs to the albite type. Subgroup E1 is the final result of magmatic differentiation, bodies of which are made up of saccharoidal albite.

During the internal evolution of these pegmatite and pegmatite – aplite bodies, the role of boron and, in some cases, phosphorus was important. Both elements promote the zoning of these bodies and the concentration of rare elements in the albitic units. In the Forcarei Sur pegmatitic field, the loss of boron to the wallrock, with the development of metasomatic tourmaline, may have led to the crystallization of the albitic units. London (1986) pointed out that the crystallization of tourmaline generates an acidic aqueous fluid; in this case, it may be responsible for the formation of the rock rich in muscovite and quartz at the contact between pegmatite bodies and their host metasediments. In group D, the role of phosphorus is important as well. This element is consumed by the formation of type-II montebrasite, which appears in the albitic unit of group-D pegmatite – aplites. The low concentration of Ca, Fe and Mn in this pegmatite – aplite-forming melt results in high activity of phosphorus and means that the montebrasite will be the Al- and Li-bearing stable phase (London & Burt 1982).

From microthermometric data and stability fields of lithium aluminosilicates and aluminosilicates, the possible conditions of emplacement of group-D pegmatite – aplites are 550°C and 3 kbars. The mixed-salt aqueous fluid (type I) that was trapped in group-D pegmatite – aplites was generated at the beginning of the albite unit's crystallization. At the same time, boron and phosphorus were consumed to form metasomatic tourmaline and type-II montebrasite. Thus, these events produce a decrease in solubility of H_2O in the melt, so that an aqueous fluid exsolved and was trapped by type-I inclusions in the group-D pegmatite – aplite. The inclusions from group-E minerals (quartz, beryl and apatite) of albitic units trapped an aqueous fluid with other volatiles (mainly CO_2 and CH_4). It is likely that this volatile-rich fluid evolved from a mixed-salt aqueous fluid due to a volatile enrichment, which could be similar to that mentioned above for group D. These volatiles may come from the host rock. Thus, the chemistry of these carbonic fluids may be controlled by graphite–fluid equilibration, implying a source for fluids external to the pegmatites (surrounding metamorphic series). Linnen & Williams-Jones (1994) proposed a similar explanation for the carbonic fluid inclusions observed in the Nong Sua aplite–pegmatite complex in Thailand. The established P–T conditions for this stage in the group-E pegmatite – aplite are around 3 kbars and greater than 440°C. Moreover, after the first stage of emplacement, the fluid inclusions of group-E pegmatite – aplite record a drop in pressure from 3 to 0.8 kbar at constant temperature of 440°C. This pressure drop may be due to the transition from predominantly lithostatic pressures to hydrostatic pressures. At that time, the fluids circulated through fractures in the pegmatitic bodies. These fractures were formed by the development of a zone of ductile shear related to the third tectonic phase that affected this pegmatite – aplite. Moreover, the inclusions in group-E pegmatite – aplite indicate the circulation of a later aqueous-carbonic fluid (stages E3) with a decrease in temperatures (minimum temperature of trapping, Th, around 360°C) at approximately constant pressure (the range of estimated pressure from a representative isochore of this type is between 0.6 to 0.75 kbar), probably due to progressive exhumation of these bodies. Finally, with a decrease in temperature (minimum temperature of trapping, Th, between 285°C and 310°C) at constant pressure (around 0.6 kbar), there is circulation of a hydrothermal aqueous fluid, which altered the pegmatite – aplite body. From the latter fluid, type-B apatite formed; this aqueous fluid transformed the phosphorus-rich feldspars into the metasomatic phosphates of these pegmatite – aplites, because this apatite appears to have corroded the albite in the albitic units.

The genetic model proposed for this type of rare-element ore (Li, Be, Nb, Ta, Sn and P) is in agreement with the zonation model from Černý (1989). The model consists of a parental granitic source and an aureole of increasingly fractionated pegmatites, with the highest concentration of rare elements in accordance with a zoned pattern about the source. The farthest bodies from the source are the most evolved.

Guidelines for the prospecting of Sn, Nb, Ta ores in Galician pegmatites may be derived from the following observations:

(1) The pegmatite bodies are genetically related to peraluminous two-mica granites, mainly of leucocratic type.

(2) The degree of fractionation of these pegmatites increases with the distance from parental granite. The more evolved bodies are mineralized. The most promising areas will be those at a greater distance from parental granite.

(3) Albite-rich pegmatite – aplites with albitic units are economically the most interesting.

(4) Wallrock tourmalinization is an important guideline in prospecting for rare-element-enriched mineralized bodies.

ACKNOWLEDGEMENTS

This work has been financed by the CICYT, project GEO 91/1077, supported by FPI of MEC fellowship to Fuertes. We acknowledge M.C. Boiron and M. Cathelineau for access to the laboratories at CREGU (Nancy, France) and for their advice and help on all aspects of Raman analysis. We thank the reviewers and editor for their encouraging suggestions, which have improved significantly the content and clarity of the paper. The authors thank Roisin Moran for reading the paper and doing a detailed correction of grammatical and spelling errors.

REFERENCES

BAKKER, R.J. (1995): The application of a computerised and optimised clathrate stability model to fluid inclusion studies. *ECROFI, Bol. Soc. Esp. Mineral.* **18**(1), 15-17.

BARRERA, J.L., FARIAS, P., GONZALEZ, F., MARQUINEZ, J., MARTIN, L.M., MARTINEZ, J.R., DEL OLMO, A. & DE PABLO, J.G. (1989): Mapa Geológico 1:200.000 de Ourense/Verín. Memoria explicativa. *Publicación I.T.G.E.*

BODNAR, R.J. (1993): Revised equation and table for determining the freezing point depression of H_2O–NaCl solutions. *Geochim. Cosmochim. Acta* **57**, 683-684.

BROWN, P.E. & HAGEMANN, S.G. (1995): Fluid inclusion data reduction and interpretation using Macflincor on the Macintosh. *ECROFI. Bol. Soc. Esp. Mineral.* **18**(1), 32-33.

ČERNÝ, P. (1989): Exploration strategy and methods for pegmatite deposits of tantalum. *In* Lanthanides, Tantalum and Niobium (P. Möller, P. Černý & F. Saupé, eds.). Springer-Verlag, Berlin, Germany (274-302).

________ (1991): Rare element granitic pegmatites. I. Anatomy and internal evolution of pegmatite deposits. *Geosci. Can.* **18**, 49-67.

________ (1994): Rare element granitic pegmatites. II. Regional to global environments and petrogenesis. *Geosci. Can., Ore Deposits Models* **2**, 49-62.

________ & BURT, D.M. (1984): Paragenesis, crystallochemical characteristics and geochemical evolution of micas in granite pegmatites. *In* Micas (S.W. Bailey, ed.). *Rev. Mineral.* **13**, 257-297.

________ & ERCIT, T.S. (1985): Some recent advances in the mineralogy and geochemistry of Nb and Ta in rare element granitic pegmatites. *Bull. Minéral.* **108**, 499-533.

________ & HAWTHORNE, F.C. (1982): Selected peraluminous minerals. *In* Granitic Pegmatites in Science and Industry (P. Černý, ed.). *Mineral. Assoc. Can., Short-Course Handbook* **8**, 136-186.

COLLINS, P.L.F. (1979): Gas-hydrates in CO_2 bearing fluid inclusions and the use of freezing data for estimation of salinity. *Econ. Geol.* **74**, 1435-1444.

CRAWFORD, M.L. (1981): Phase equilibria in aqueous fluid inclusions. *In* Fluid Inclusions: Applications to Petrology (L.S. Hollister & M.L. Crawford, eds.). *Mineral. Assoc. Can., Short-Course Handbook* **6**, 75-100.

DUBESSY, J. (1984): Simulation des équilibres chimiques dans le système C–O–H. Conséquences méthodologiques pour les inclusions fluides. *Bull. Minéral.* **107**, 157-168.

________, POTY, B. & RAMBOZ, C. (1989): Advances in the C–O–H–N–S fluid geochemistry based on micro-Raman spectroscopic analysis of fluid inclusions. *Eur. J. Mineral.* **1**, 517-534.

________, THIERY, R. & CANALS, M. (1992): Modelling of phase equilibria involving mixed gas clathrates. Application to the determination of molar volume of the vapour phase and of the salinity of the aqueous solution in fluid inclusions. *Eur. J. Mineral.* **4**, 873-884.

EL-BOUSEILY, A.M. & EL-SOKKARY, A.A. (1975): The relation between Rb, Ba and Sr in granitic rocks. *Chem. Geol.* **16**, 207-219.

FARIAS, P., GALLASTEGUI, G., GONZALEZ LODEIRO, F., MARQUÍNEZ, J., MANTIN PARRA, L.M., PABLO MACIA, J.G. DE & RODRIGUEZ FERNANDEZ, L.R. (1987): Aportaciones al conocimiento de la litoestratigrafia y estructura de Galicia Central. *Mem. Fac. Cienc. Univ. Porto* **1**, 411-431.

FUERTES-FUENTE, M. & MARTIN-IZARD, A. (1994): El campo pegmatítico de Forcarey y las mineralizaciones de Sn, Ta, y Nb asociadas (Pontevedra, Galicia, España). *Bol. Soc. Esp. Min.* **17**, 51-63.

________, ________ & MOREIRAS, D. (1995): The Forcarei Sur zoned pegmatitic field, Galicia, northwestern Spain. *In* Mineral Deposit (J. Pašava, Kribek & Žák, eds.). Balkema, Rotterdam, The Netherlands (439-442).

GALLEGO GARRIDO, M. (1992): *Las mineralizaciones de litio asociadas al magmatismo ácido en Extremadura y su encuadre en la zona Centro Ibérica.* Ph.D. thesis, Univ. Complutense de Madrid, Madrid, Spain.

HENSEN, B.J. (1967): Mineralogy and petrography of some tin – lithium and beryllium bearing albite pegmatites near Doade, Galicia (Orense). *Leidse Geol. Med.* **36**, 249-259.

JACOBS, G.K. & KERRICK, D.M. (1981): Methane: an equation of state with application to the ternary system H_2O–CO_2–CH_4 system. *Geochim. Cosmochim. Acta* **45**, 607-614.

KERRICK, D.M. & JACOBS, G.K. (1981): A remodified Redlich – Kwong equation for H_2O–CO_2 and H_2O–CO_2–NaCl mixtures at elevated pressures and temperatures. *Am. J. Sci.* **281**, 735-767.

KRETZ, R. (1983): Symbols for rock-forming minerals. *Am. Mineral.* **68**, 277-279.

LINNEN, R.L. & WILLIAMS-JONES, A.E. (1994): The evolution of pegmatite – hosted Sn–W mineralization at Nong Sua, Thailand: evidence from fluid inclusions and stable isotopes. *Geochim. Cosmochim. Acta* **58**, 735-747.

LONDON, D. (1984): Experimental phase equilibria in the system $LiAlSiO_4$–SiO_2–H_2O: a petrogenetic grid for lithium-rich pegmatites. *Am. Mineral.* **69**, 995-1004.

________ (1986): Magmatic–hydrothermal transition in the Tanco rare element pegmatite: evidence from fluid inclusions and phase-equilibrium experiments. *Am. Mineral.* **71**, 376-395.

________ & BURT, D.M. (1982): Lithium minerals in pegmatites. *In* Granitic Pegmatites in Science and Industry (P. Černý, ed.). *Mineral. Assoc. Can., Short-Course Handbook* **8**, 99-133.

MARQUÍNEZ, J. (1984): La geología del Area Esquistosa de Galicia Central (Cordillera Herciniana, NW de España). *Mem. del I.G.M.E.* **100**, 1-213.

MARTÍNEZ CATALÁN, J.R., ARENAS, R., DIAZ GARCIA, F., RUBIO PASCUAL, F.J., ABATI, J. & MARQUÍNEZ, J. (1996): Variscan exhumation of a subducted Paleozoic continental margin: the basal units of the Ordenes Complex, Galicia, NW Spain. *Tectonics* **15**(1), 106-121.

MATTE, P.H. (1968): La structure de la virgation hercynienne de Galicia (Espagne). *Trav. Lab. Géol. Fac. Sci. Grenoble, Revue de Géol. Alpine* **44**, 1-128.

MONTERRUBIO, S. (1991): *Mineralizaciones asociadas a rocas ultrabásicas en el hercínico español.* Ph.D. thesis, Univ. Complutense de Madrid, Madrid, Spain.

MOORE, P.B. (1982): Pegmatite minerals of P(V) and B(III). *In* Granitic Pegmatites in Science and Industry (P. Černý, ed.). *Mineral. Assoc. Can., Short-Course Handbook* **8**, 267-291.

PARASKOVOPOULOS, G.M. (1953): Beitrag Zur Kenntnis der Feldspate der Tessiner Pegmatite. *Tschermaks Mineral. Petrogr. Mitt.* **3**(3), 191-271.

PARGA PONDAL, I. & MARTÍNEZ CARDOSO, G. (1948): Die Lithium-pegmatite von Lalín, Prov. Pontevedra, Galizien. *Schweiz. Mineral. Petrogr. Mitt.* **28**, 324-334.

POTTER, R.W. & BROWN, D.L. (1977): The volumetric properties of aqueous sodium chloride solution from 0°C to 500°C at pressures up to 2000 bars based on a regression of available data in the literature. *U. S. Geol. Surv., Bull.* **1421-C**, 1-36.

POTY, B., LEROY, J. & JACHIMOWICZ, L. (1976): Un nouvel appareil pour la mesure des températures sous le microscope, l'installation de microthermométrie Chaixmeca. *Bull. Soc. fr. Minéral. Cristallogr.* **99**, 182-186.

ROBIE, R.A. & HEMINGWAY, B.S. (1984): Entropies of kyanite, andalusite and sillimanite: additional constraints on the pressure and temperature of the Al_2SiO_5 triple point. *Am. Mineral.* **69**, 298-306.

ROEDDER, E. (1984): Fluid inclusions. *Rev. Mineral.* **12**.

SHEPHERD, T.J., RANKIN, A.H. & ALDERTON, D.H.M. (1985): *A Practical Guide to Fluid Inclusion Studies.* Blackie & Son Ltd., London, U.K.

SWANENBERG, H. (1979): Phase equilibria in carbonic systems and their aplication to freezing studies of fluid inclusions. *Contrib. Mineral. Petrol.* **68**, 303-306.

THIERY, R., VIDAL, J. & DUBESSY, J. (1994): Phase equilibria modelling applied to fluid inclusions: liquid – vapor equilibria and calculations of the molar volume in the CO_2–CH_4–N_2 system. *Geochim. Cosmochim. Acta* **58**, 1073-1082.

WINKLER, H.G.F. (1976): *Petrogenesis of Metamorphic Rocks.* Springer-Verlag, New York, N.Y.

WISE, W.S. & LOH, S.E. (1976): Equilibria and origin of minerals in the system Al_2O_3–$AlPO_4$–H_2O. *Am. Mineral.* **61**, 409-413.

WOOD, S.A. & WILLIAMS-JONES, A.E. (1993): Theoretical studies of the alteration of spodumene, petalite, eucryptite and pollucite in granitic pegmatites: exchange reactions with alkali feldspars. *Contrib. Mineral. Petrol.* **114**, 255-263.

YARDLEY, B.W.D. (1989): *An Introduction to Metamorphic Petrology.* Longman, Essex, U.K.

YPMA, P.J.M. (1966): Structural petrology of an area near Santiago de Compostela. (NW Spain). *Leidse Geol. Med.* **45**, 1-71.

ZHANG, Y.G. & FRANTZ, J.D. (1987): Determination of the homogenization temperatures and densities of supercritical fluids in the system NaCl–KCl–$CaCl_2$–H_2O using synthetic fluid inclusions. *Chem. Geol.* **64**, 335-350.

Received March 22, 1997, revised manuscript accepted January 26, 1998.

APPENDIX: ANALYTICAL TECHNIQUES

Petrographic examinations were made using transmitted- and reflected-light polarizing microscopes. For mineral identification, we also used X-ray powder diffraction. The Philips PW 1729/1710 diffractometer was used with Cu$K\alpha$ radiation at 40 kV and 30 nA. Some minerals were analyzed with a CAMEBAX SX–50 electron microprobe (with international standards). In all cases, the standard deviation of results is less than 5%. Concentrations of the light elements have been calculated by stoichiometry. Electron-microprobe analyses were performed at University of Oviedo (Spain) and University Paul-Sabatier (Toulouse, France). The beam conditions were 15 kV and 15 nA for the most of mineral analyses. For the analysis of cassiterite, columbite – tantalite and zircon, the beam conditions were changed to 20 kV and 10 nA. In the case of analysis of minerals for fluorine, the conditions were changed to 10 kV and 15 nA. The following international standards were used: ALB1, ORTH, ALBI, FE2O, MNTI, ANDO, MGO, CR2O, MNTI, NIO, APATITE, synthetic Ta_2O_5, synthetic $MnWO_4$, synthetic SnO_2, niobium, zircon, synthetic HfO_2.

In the geochemical study, bodies characterized by weak hydrothermal alteration, representative of the different pegmatite groups, were chosen. The samples were taken from all zones of these bodies, and the grain-size of the body was taken into account. Thus the samples from fine-grained zones were more numerous than the samples from coarse-grained zones. The whole-rock samples weighed about 15–20 kg. Moreover, muscovite-rich zones of the bodies were sampled to extract this mineral. The muscovite samples were prepared by flotation or hand-picking, and the separates were examined with a binocular microscope to remove contamination. Major- and trace-element analyses of whole rocks and muscovite were performed in Canada at ACME Analytical Laboratories Ltd. and ACTLABS Activation Laboratories Ltd. Whole-rock concentrations of SiO_2, Al_2O_3, Fe_2O_3 (as total iron), MgO, CaO, Na_2O, K_2O, TiO_2, P_2O_5, MnO, Cr_2O_3, Li, Be, Sn and Nb were established by inductively coupled plasma (ICP). Samples (0.2 g) are fused with 1.2 g of $LiBO_2$ and dissolved in 100 mL 5% HNO_3. Concentrations of Rb, Cs and Ta were established by instrumental neutron-activation analysis (INAA). The detection limits are: for all oxides 0.01%, Li 2 ppm, Be 1 ppm, Sn and Nb 2 ppm, Rb 5 ppm, Cs 1 ppm and Ta 0.5 ppm. Concentrations of Fe, Na, Sn, Mn, Ca, P, Al, K, Nb, Li and Mg in muscovite were established by ICP, and concentrations of Cs, Rb, Ta and Zn, by INAA. The detections limits are: Fe, Al, Ca, Na, K and Mg 0.01%, P 0.002%, Li, Sn and Nb 2 ppm, Mn and Rb 5 ppm, Cs 1 ppm and Ta 0.5 ppm. All sample preparations were carried out at the University of Oviedo. In whole-rock samples, 0.5 kg of rock was reduced to 3–4 mm by crushing, and 100 g was pulverized to at least 150 mesh in a mild steel to minimize Cr contamination. In muscovite samples, 10 g was pulverized to at least 150 mesh in an agate mortar.

Microthermometric studies of fluid inclusions were performed on 300-μm thick sections using a microscope equipped with a UMK50 Leitz objective and a Chaixmeca cooling and heating stage (Poty *et al.* 1976) in the Laboratory of Fluid Inclusions of Oviedo (Spain) and Laboratory of Geology of the University of Las Palmas (Spain). The stage was calibrated according to procedures outlined by Poty *et al.* (1976). The volumetric fraction of the volatile-rich phase (Vg/Vl) was estimated by reference to the volumetric chart of Roedder (1984). Salinity is expressed in equivalent wt% NaCl (Bodnar 1993) and wt% $CaCl_2$ (Zhang & Frantz 1987). Fluid density of volatile-free inclusions was determined by microthermometry (Potter & Brown 1977, Zhang & Frantz 1987). In dense volatile fluid inclusions, CO_2 was identified by the melting a solid below –56.6°C. In inclusions with a low-density volatile phase, the presence of a volatile phase (CO_2 or CH_4) was identified by the melting of hydrates in suitable cases, or by Raman microprobe. Gas hydrate was detected in the inclusions by the presence of a double freezing event during cooling (hydrate and ice: Collins 1979). However, as only small amounts of hydrate formed, it was impossible to observe hydrate melting directly. In order to determine the melting temperature of the hydrate as accurately as possible, a freeze – refreeze technique was used (Roedder 1984, Shepherd *et al.* 1985). This technique involves raising the temperature of the inclusion to a fixed point (*e.g.*, 10°C), and then freezing it again rapidly. If any solid clathrate remains in the inclusion, a solid phase will grow back immediately on cooling, resulting in shrinkage and "squashing" of the vapor bubble. When a temperature is reached at which no further deformation of the vapor bubble occurs on quenching, then the measurements were made with a precision of ±0.5°C. As will become clear from the calculations of salinity, it is necessary to determine the melting point of the hydrate as precisely as possible.

The composition of the non-aqueous portion of individual inclusions was measured using a Dilor X–Y multichannel modular Raman spectrometer (at CREGU). Bulk composition and density were computed from the P–V–T–*X* properties of individual inclusions in the system C–O–H–(N–S) (Dubessy 1984, Dubessy *et al.* 1989, 1992, Thiery *et al.* 1994, Bakker 1995). All data were calculated from the microthermometric measurements and the Raman gas analyses, using a clathrate stability model in the fluid system H_2O–CH_4–N_2–NaCl–KCl–$CaCl_2$, between 253 and 293 K and between 0 and 200 MPa (Bakker 1995) and the computer program of Bakker (1995).

The P–V–T–*X* properties of aqueous carbonic inclusions were modeled for the system H_2O–CO_2–CH_4 using the equations of state of Kerrick & Jacobs (1981) and Jacobs & Kerrick (1981) and the computer code of Dubessy (1984). For aqueous inclusions, the isochores have been drawn in the systems H_2O–NaCl and H_2O–$CaCl_2$ using data from Zhang & Frantz (1987) and the computer program Macflincor 0.92 (Brown & Hagemann 1995).